The Plymouth Student Scientist, 2020, **13**, (1), 253-289

Oscillations of Cantilevered Tubular Steel Piles in Current Flow

Matthew House

Project Advisor: Jon Miles, School of Engineering, University of Plymouth, Drake Circus, Plymouth, PL4 8AA

Abstract

A laboratory experiment was conducted in a 20 m flume tank at Plymouth University to investigate the movement of, and forces applied to, a pair of in-line cantilevered piles. 2-minute tests were run with a 64 mm diameter upstream pile and downstream piles of 64 mm, 40 mm and 30 mm. Current velocities ranging from 0.1 to 0.9 m/s and spacings between the piles of 3 to 10 diameters were varied along with the downstream pile diameter. Initially, tests with all 3 piles on their own were conducted and the results showed a close comparison with the theoretical cross-flow oscillation frequency and the measured cross-flow oscillation frequency of the solitary pile. Similarities between the theoretical and measured steady drag forces were not identified but a significant relationship between steady drag force on the downstream pile and spacing was discovered. The results indicated that when the spacing was small, approximately 3 to 4 diameters, the downstream pile experienced more drag force than the upstream. The force steadily decreased until it appeared to level out around 9 to 10 diameters away. Analysis of the cross-flow oscillations of the downstream pile revealed that the 64 mm pile oscillated with a frequency close to the theoretical at all spacings and flow velocities. Whereas, the 40 mm and 30 mm piles oscillated with frequencies less than the theoretical, at all spacings and flow velocities. Despite the solitary 40 mm and 30 mm piles oscillating at the theoretical frequency. This demonstrated that the oscillation frequency of the downstream pile was governed by the size and therefore the vortex shedding frequency of the upstream pile.

Introduction

A pile is a vertical element that can be used in the foundations of many small or large structures. Piles can range from pieces of timber of less than 100 mm across to substantial steel cylinders with diameters of over 5 m. Piles are often used in construction as they can efficiently transfer large loads deep into the ground where soil conditions are typically good and are able to effectively resist loads. Alternatively, shallow foundations can be used but the ground must be excavated to position them, and soil conditions are generally weaker nearer the surface. Whereas piles are driven straight into the ground.

Maritime structures all over the world, including; jetties, quays, ports and offshore structures use piles as their foundations.
In the UK, approximately 96% of the volume of imports and exports leave and enter the country on ships, as well as over 70 million passengers using them for domestic and international journeys (UK Ports, 2018). Although much of the trade is handled by a select number of ports, lots of the liquid and dry bulk tonnage is passed through jetties and offshore structures, commonly located in estuaries such as the Port of Immingham and the Port of Milford Haven. The department for transport (2017) states that, “In 2017 189.1 million tonnes of liquid bulk were handled by UK major ports”. Which, although slightly less than in previous years, still accounts for 40% of all tonnage.

Much of the port and maritime work in the UK is upgrading and maintenance to existing structures, rather than the development of brand-new ones. However, the statistics are evidence that the construction and upkeep of UK port and jetty infrastructure is vital. The design and construction of structures in the marine environment is notoriously difficult; wave, current, tidal and ground conditions all impose challenges that must be considered to ensure structures remain safe and operational. The Defence Infrastructure Organisation (DIO) has recently awarded a contract worth £43m for the construction of a new fuel jetty at its Thanckes Oil Depot on the banks of the river Tamar in Plymouth (McDonald, 2017). The project requires the demolition and replacement of the existing Yonderberry Jetty, which provides fuelling facilities for Royal Navy ships based at Devonport Naval Base and to other customers.

Construction of the new jetty began in late 2018 with the driving of the steel piles that make up the foundations of the almost 200 m long jetty approach and the 80 m long x 14 m wide jetty head elements (Jacobs, 2018a). An area of interest surrounding the design of cylindrical piles is the generation of cyclic loading caused by the shedding of vortices. The vortices can be generated by currents from the flow of a river/estuary or from currents generated by tides, which is common in many UK ports situated in large river mouths, like Immingham and Milford Haven. The vortex induced vibrations could lead to an unfavourable harmonic response of the structure which, if of a high enough magnitude, can lead to substantial damage or even failure.

The UK standard for maritime design, BS 6349 (BSI, 2016) outlines guidance for designing piles against loadings from waves and currents. To ensure that a harmonic response does not occur, the natural frequency and hence critical flow velocity of a pile must not match the velocity of the flow. However, the resonant frequency of piles is different during the construction phase and when a structure has been finished.

During construction, piles are generally in a cantilevering position until the main deck and beam elements are placed on top.

It is during this condition that this report will focus on, with the aim of understanding in greater detail the movement and oscillations of piles during the typical construction phase. More specifically, how the oscillations of a pair of in-line piles vary with current velocity, separation and pile diameter in both cross-flow and in-line directions. It is critical that these conditions are well understood to prevent damage and failure of some of the UK's most essential trade infrastructure.

Literature Review

Current Flow and Forces around Cylindrical Structures

Current forces on piles and other submerged structures are a key element of maritime and coastal engineering design. They are often overlooked as wave forces can produce higher loads, especially on large offshore structures i.e., oil platforms but, as discussed, the consequences of ignoring them could be serious.
The British Standards Institution (BSI) (2016) present the steady drag force equation (**Equation *(1)***) for calculating the force on submerged piles of different materials and sizes due to current.

$$F_D = \frac{1}{2}(C_D \rho u^2 A_n) \qquad \textit{(1)}$$

Where;

F_D is the steady drag force, in Newtons (N);
C_D is the dimensionless drag coefficient;
ρ is the mass density of water, in kilograms per cubic metre (kg/m^3);
u is the current velocity, in metres per second (m/s);
A_n is the area of the member normal to flow, in square metres (m^2).

The drag coefficient, C_D is dependant upon the Reynolds number and the surface roughness of the member, with rougher surfaces generally resulting in larger values of C_D.
The drag coefficient can range from an approximate maximum of 1.2 to a minimum of approximately 0.2 for a member with a relative roughness, k/D of 0.

Where;

k is the roughness of the member;
D is the diameter of the member.

Hence, the drag coefficient can cause an increase in current loading by a factor of 6. Although the steady drag equation is a simple formula, Tomlinson and Woodward (2007) discuss the idea that the current force should be worked out more accurately by calculating the force at height increments above the seabed. This provides a more realistic result as the current velocity is not always uniform in any depth of water. If sea and river beds are cluttered with rocks and vegetation, velocities are likely to be much lower than in the central region of flow due to the effective drag imposed on the water by the bed. The relationship between flow velocity and

distance from the bed can be characterised by a logarithmic profile (Soulsby, cited in Whitehouse 1998) where the flow velocity increases with distance from the bed due to the bottom boundary layer.

Usually, relative to the overall water depth, the bottom boundary layer is thin. Therefore, the flow velocity on submerged elements is fairly uniform. Crowdy (2006) discusses the basic problem of uniform flow past multiple circular cylinders and how the topic has been of interest to fluid dynamicists for many years. According to Crowdy, the earliest investigations into flow around 2 cylinders are by Hicks (1879) and Greenhill (1882). Crowdy converses in detail about the mathematical solution for flow around multiple cylinders, however it only provides an analytical solution rather than a simple expression for force, making it not an appropriate paper to use as a comparative source.

Vortex Shedding and Flow Induced Oscillations

Strouhal Number

The Strouhal number, S is a dimensionless number that is commonly used to predict the vortex shedding frequency. The formula for the Strouhal number is presented below as **equation *(2)*** (Sunden, 2011).

$$S = 0.198\left(1 - \frac{19.7}{Re_D}\right) \quad \textit{(2)}$$

Where;

$\mathrm{Re_D}$ is the pile Reynolds number.

Alternatively, if the Strouhal number has been calculated using **equation *(2)***, **equation *(3)*** can be used to calculate the frequency of vortex shedding.

$$S = \frac{f_s D}{U_\infty} \quad \textit{(3)}$$

Where;

S is the Strouhal number;
$\mathrm{f_s}$ is the vortex shedding frequency, in Hertz (Hz);
D is the pile diameter, in metres (m);
U_∞ is the freestream velocity, in metres per second (m/s).

As shown, the Strouhal number is directly related to the Reynolds number, which varies with flow velocity. Due to the nature of **equation *(2)***, the Strouhal number is mostly affected at lower Reynolds numbers i.e. between 20 and 1000. At higher values of Reynolds number, the equation effectively becomes $S = 0.198(1 - 0) = 0.198$. The Reynolds number for flow around a pile is calculated with **equation (4)** below (Miles et al, 2017):

$$Re_D = \frac{U_\infty D}{\nu} \quad \textit{(4)}$$

Where;

Re_D is the pile Reynolds number;
U_∞ is the freestream velocity, in metres per second (m/s);
D is the pile diameter, in metres (m);
ν is the kinematic viscosity of the fluid, in square metres per second (m^2/s).

If calculating the Reynolds number in an open channel, D is replaced by the hydraulic radius, R. Reynolds numbers of river and estuary flows are usually in the order of 500000+ (Fowler, 2011). Therefore, the Strouhal number and hence the frequency of eddy shedding is highly dependent on the pile diameter and flow velocity.

Flow Induced Oscillations
Flow induced oscillations, or vibrations, are a known phenomenon that need to be accounted for in the design of maritime structures. As discussed, the natural frequency of slender elements can be matched by the vortex shedding frequency, which can lead to oscillations of a large magnitude. Mittal and Kumar (2001) conducted a computational experiment on a pair of tandem and staggered piles. The piles were separated by 5.5 times the cylinder diameter and they investigated movement of the downstream pile due to the wake caused by the oscillations of the upstream pile. They found that the trajectory of the upstream pile resembled a figure of eight pattern as it was acting as a solitary pile while the downstream pile experienced a different movement pattern due to the interference from the upstream pile, especially in the staggered case. The results are interesting, however not entirely appropriate for this report, as an extremely low Reynolds number of 100 was used. This leads to much more organised and predictable wake and vortex effects, which cannot be achieved with a Reynolds number > 10000.

Meanwhile, Miles et al (2017) conducted an experiment investigating the wave and current effects in the vicinity of a wind turbine monopile. The scale of Miles' model was based on a relevant prototype depth of 12.5 m and the fixed depth of the wave basin where the experiment was being conducted. With a scale ratio of 25, a 0.2 m pile was used to represent a prototype monopile with a diameter of 5.0 m. Miles' results showed that the current velocity returned to within 5% of the background value approximately 8.3 diameters downstream and had returned to full flow by 10.5 diameters. This implies that a downstream pile placed 10.5 diameters away would experience the same current force as the upstream pile, and therefore should follow the same oscillation pattern.

In a similar experiment to Miles' (2017), Xu and Zhou (2004) investigated the variation of Strouhal number near a pair of in-line piles. The pair discovered that no vortex street formed when the gap between both piles was less than the critical value, which ranged from $3.5(L/d)$ to $5(L/d)$. Where L is the centre to centre spacing and d is the pile diameter. Whereas, when the distance between the 2 piles was greater than the critical distance, co-shedding started to occur. This is when vortices are shed from both the upstream and downstream cylinders. Comparable results were found by Okla et al. (1972). He discovered that vortex shedding did not occur until $L/d > 3.8$, which is within the critical range found by Xu and Zhou. Xu's investigation is relevant to this report as Reynolds numbers of 800 to 42000 were

used, therefore the results were found using turbulent flow, rather than more predictable laminar flow.

Immingham Oil Terminal Pile Oscillation Failure

The Port of Immingham is located west of Grimsby on the south bank of the river Humber. The construction of the original dock was completed in 1912 and was largely used for the exportation of coal. Construction and opening of the oil terminal expansion was in 1969. Today, the oil terminal serves as the main location in the UK for the importation of oil (Mwaniki, 2018) and the port is the busiest by tonnage, in the UK, handling 54.0 million tonnes in 2017 (UK Ports, 2018).

As presented by Sainsbury (1971), the oil terminal stretches more than half a mile into the estuary, to water with a mean depth of roughly 23 m, where spring tides can reach velocities of over 2.6 m/s. The jetty consists of helically welded piles, 610 mm and 762 mm in diameter with thicknesses of 12.7 mm, which unfortunately experienced very severe oscillations during construction. The oscillations reached magnitudes of up to 1.2 m, which ultimately lead to the failure of some of the piles (Tomlinson and Woodward, 2007). Many of the piles failed on or just above the seabed soon after they had been driven. The driven piles, in a cantilevered position had not yet been braced. This most likely would have reduced the severity of the oscillations.

At the time, the resonant oscillation of cylindrical structures in air was well known to engineers. Similar effects in water had been recognised as phenomena or reported as design considerations, as noted by Scruton and Flint (1964). But, the problem of vortex induced oscillations was not fully understood and therefore unforeseen during the design. Tomlinson and Woodward (2007) reiterate the necessity of determining the natural frequency and critical velocity of the piles and current flow, especially for structures in a cantilevering condition during the construction phase of a project. The aim of this report is to identify how the cross-flow oscillations and in-line steady drag force on a pair of cantilevered piles is affected by the spacing between them, and how this is affected by changing the diameter of the downstream pile to a smaller size than the upstream pile.

Methodology

The main challenge was designing a system that would be able to record the current forces and oscillations of piles that could be placed in water and moved around. Small electronic strain gauges were used to measure the stress at the fixing point of the piles. The gauges were calibrated to convert the output change in voltage to a force experienced by the piles. The decision was taken to suspend the piles from above the water rather than have them fixed at the bed of the tank. This avoided having to waterproof any electronics that would have needed to be in the water. Fixing the piles from the top meant that the wiring of the strain gauges was much simpler.

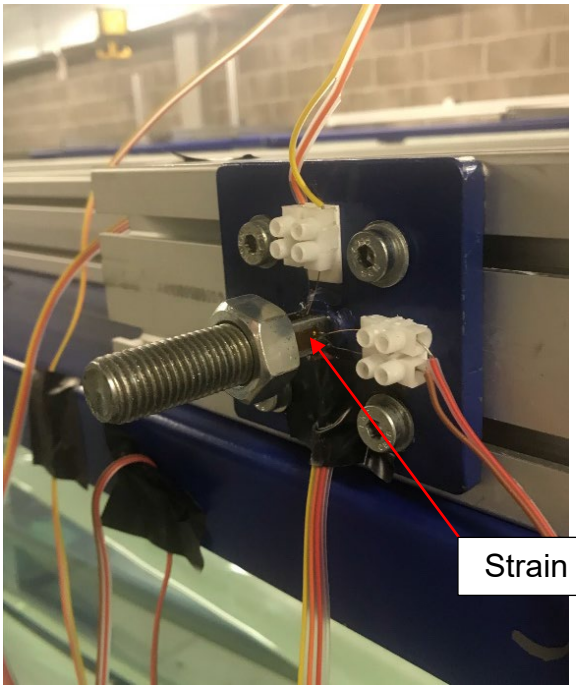

Figure 1: Attachment for the top of the piles.

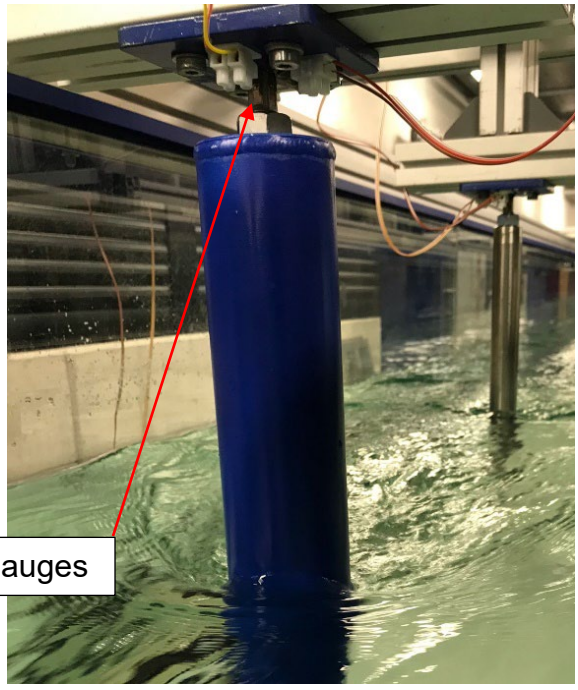

Figure 2: Pile fixed to the attachment and placed into the flume.

Figure 1 shows the attachment for the pile that was created. It consisted of a steel plate with 4 holes, so it could be bolted to the MiniTec aluminium bars, a 12 mm thread that the piles were screwed on to and a section of steel in between for the strain gauges to be glued to. **Figure 2** shows a pile attached and being suspended into the flume.

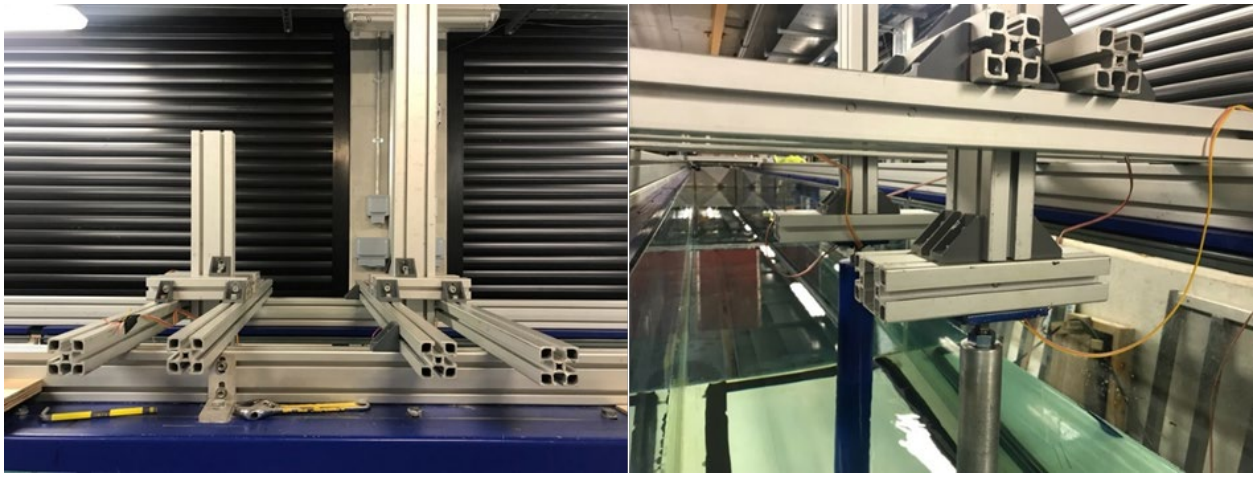

Figure 3: Final set up of the experiment.

Figure 3 displays the final set up of the MiniTec bars and how the piles and strain gauge attachments were assembled. The set-up was able to be easily adjusted so the distance between the piles could be changed between runs.

Equipment

The experiment was conducted over 5 days in a flume tank in Plymouth University's Marine Building. The 20 m long tank can produce currents > 1 m/s with water depths up to 0.8 m. The flume is shown in **Figure 4**.

Figure 4: 20 m flume tank in the Plymouth University Marine Building.

The strain gauges used were 'Omega precision SGD-5/350-LY11 strain gages'. The linear gauges have a broad working temperature range and are less than 10 mm in length, so could be attached to the pile fixings easily. The gauges were wired up to a national instruments box (**Figure 5**) with a sampling frequency of 1612 Hz.

Figure 5: National instruments boxed wired to the strain gauges.

Figure 6: Valeport impeller used to measure the current speed.

A Valeport open channel flow meter, shown in **Figure 6**, was used to measure the current velocity in the flume. The impeller can record current speeds from 0.5 to 5.0 m/s and with a diameter of 50 mm, could easily be used in shallow water. The

impeller recorded the flow velocity for 60 seconds and calculated an average that was displayed on a digital screen.

Scaling

The scale of the model was loosely based on dimensions of the Thanckes Oil Fuel Jetty. The main Jetty head piles are situated in roughly 12.5 m of water. A water depth of 0.5 m was used in the flume, so a scale ratio of $12.5/0.5 = 1:25$ was used. **Table 1** presents the dimensions of some of the piles and current conditions at the Thanckes jetty (Jacobs, 2018b), the corresponding dimensions of the model based on a 1:25 scale ratio and the model dimensions that were chosen.

Table 1: Dimensions of the Thanckes Jetty piles and the chosen dimensions of the model piles.

Dimension	Unit	Thanckes Jetty	1:25 Scale Dimensions	Selected Dimensions
Pile Diameter	(mm)	1524	60.96	64
		1067	42.68	40
		711	28.44	30
Pile Length	(m)	17	0.68	0.70
Current velocity	(m/s)	0.67	0.13	0.1 - 0.9

The exact 1:25 scale dimensions were not chosen for the model due to the availability of materials. However, the diameter and length of the piles that were adopted are close enough to give a good representation of the real jetty. The current velocity of the model was calculated by Froude scaling the velocity at the Thanckes site in the river Tamar. Although, to extend the applicability of the observations a range of current velocities were used in the experiment.

Calibration

Current Velocity

The flume's current pump needed to be calibrated as it worked on a water depth percentage basis. Therefore, if the pump was set to 50% with a water depth of 0.3 m, the flow velocity will not be the same as for a depth of 0.5 m. The current velocity was calibrated using the Valeport impeller by measuring the current velocity at known pump percentages to create a calibration graph that could be translated to a pump percentage for a required current velocity. The results of the velocity calibration are presented in **Figure 7**.

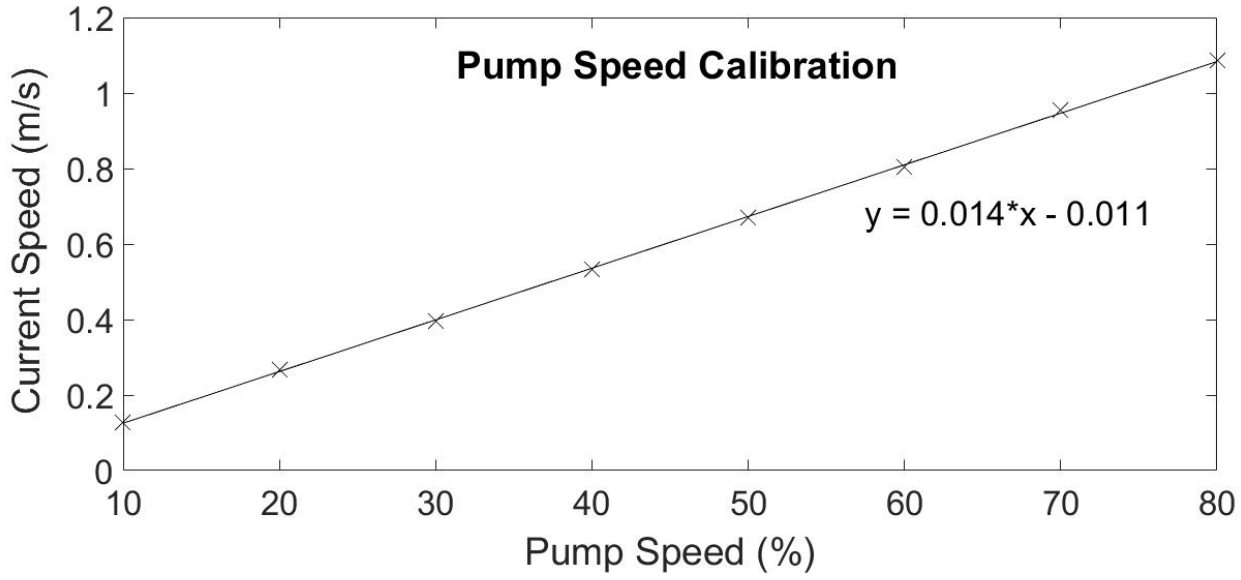

Figure 7: Current velocity calibration graph.

Table 2 presents the pump percentage required to achieve current velocities of 0.1, 0.3, 0.5, 0.7 and 0.9 m/s using the equation of the trend line from **Figure 7**.

Table 2: Required pump speed for current velocity based on the calibration equation.

Required Velocity (m/s)	**Pump Speed** (%)
0.1	8.1
0.3	22.7
0.5	37.3
0.7	51.9
0.9	66.5

Velocity Depth Profile

As discussed in 0, Tomlinson and Woodward (2007) recommend that when using the steady drag equation, the force should be calculated at increments along the length of the pile, as often the current velocity can change with depth. However, for this experiment, the boundary conditions are likely to be very thin due to the glass sides and base of the flume having a very low relative roughness.

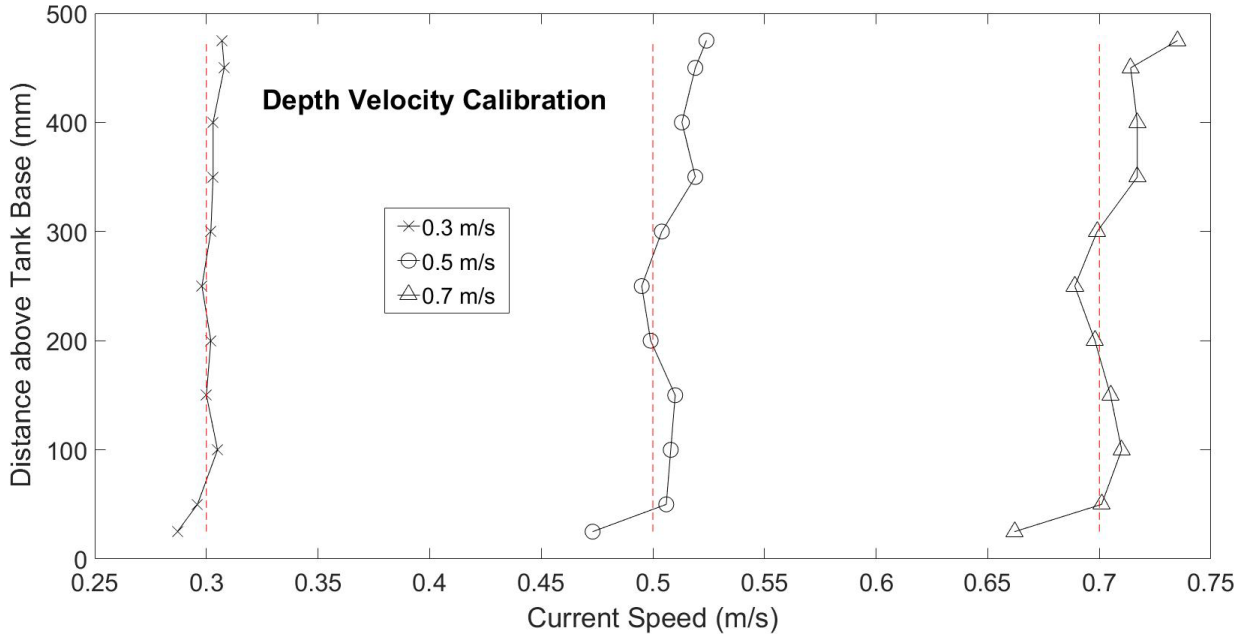

Figure 8: Depth velocity profile for 3 different current velocities.

A depth velocity calibration was also conducted on the first day of testing and the results are presented in **Figure 8**. The velocity was measured at 50 mm increments in the flume with 3 different flow velocities, 0.3, 0.5 and 0.7 m/s. **Figure 8** shows that the velocity profile is almost uniform throughout the entire depth of the flume. At the base of the tank, for all 3 flow velocities, the current is slower, although this was too be expected because of the small boundary layer. The difference in velocity is no more than 5.4% of the original velocity, so for this experiment, the depth velocity relationship has been presumed to be constant. The implications this had on the results of the testing is that the current force is effectively applied half way along the submerged section of the pile, as illustrated by **Figure 10**.

Figure 9: Changing the depth of the Valeport Impeller during the depth velocity calibration.

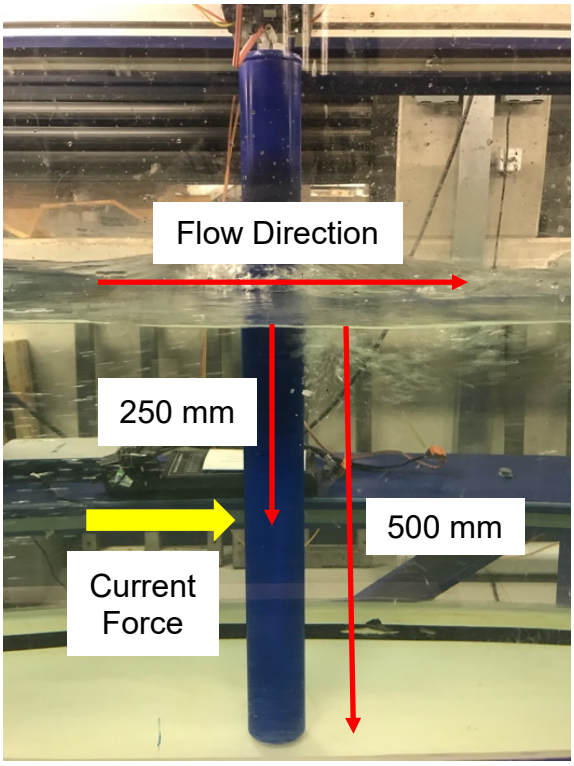

Figure 10: Location that the current force is applied to pile due to a uniform velocity depth profile.

Strain Gauges

Force exerted on the piles caused the attachment and hence the strain gauges, to bend slightly, which changed the resistance through the circuit in the electronic gauges. This results in a variation in voltage over time output from the gauge, which needs to be converted to a force.

Figure 11: Adding weight to the pile during the strain gauge calibration.

The calibration consisted of hanging a known mass from the pile (see Figure 11) and recording the change in voltage. The masses were hung 250 mm from the end of the pile, as this was representative of the drag force being applied half way along the submerged element. **Figure 12** and **Figure 13** present the calibration graphs and equations for both the upstream and downstream pile. Calibration was conducted for both pile attachments as the length of steel that that gauges were fixed to on each pile attachment was slightly different, meaning that with the same force applied, the gauges would show different changes in voltage. This resulted in different calibration equations for both piles.

As shown in **Figure 12** and **Figure 13** the calibration equations for transforming the voltage to mass exerted on the pile are $y = 15216x + 216.7$ and $y = -14349x - 221.83$ for the downstream and upstream pile attachments respectively.

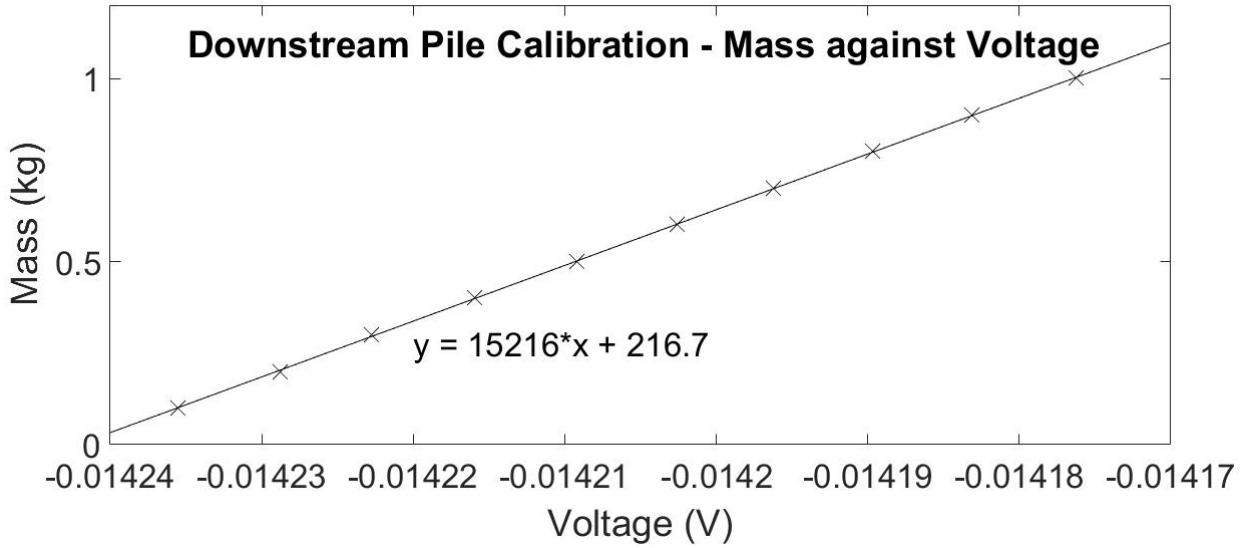

Figure 12: Results from the calibration of the downstream pile.

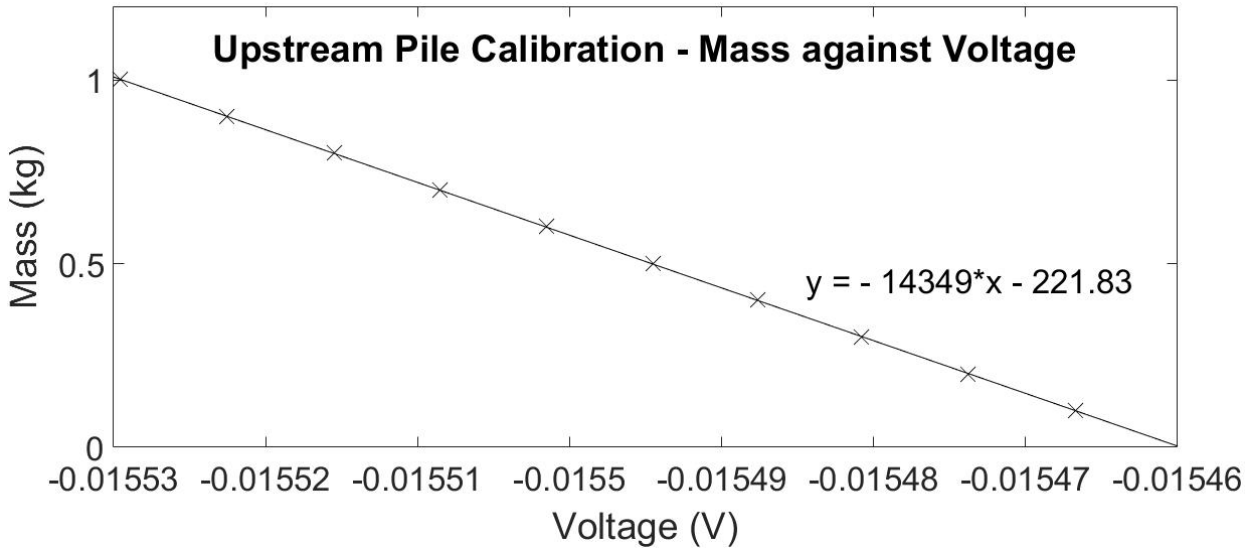

Figure 13: Results from the calibration of the upstream pile.

Testing

A systematic run matrix was created that presents all the individual test runs that were completed. Each test involved changing the current velocity, the spacing between the 2 piles or the diameter of the downstream pile. Although 3 different sized piles were used, the upstream pile remained at 64 mm, while the downstream piles were changed for the other sizes, 40 mm and 30 mm.
Between each test, the spacing between the piles was increased by 1 diameter, i.e. 64 mm. Pieces of plywood cut to lengths of 64 mm, 128 mm, 196 mm etc. were used to measure the spacing between the piles due to the difficulty of measuring the distance with a ruler. This is demonstrated in **Figure 14**. Spacings of 3 - 10 diameters were tested, smaller spacings of 1 and 2 diameters were not able to be tested because the MiniTec bars and set up of the experiment restricted the piles from being very close to each other.

When the downstream pile was replaced with a pile of a different diameter, most of the MiniTec bars needed to be loosened and lifted to allow the pile to be unscrewed from the attachment and the new one reattached. On occasion, once the new pile was attached it was noticed that it was not completely vertical. The piles were forced to vertical once they had been attached and a digital protractor was used to ensure that the piles were completely straight, as shown in **Figure 15**.
To ensure that the piles could oscillate, they could not be touching the base of the flume. Instead, when the piles were attached they were lowered onto a piece of 3 mm thick plywood. This was removed after the rig had been tightened and the pile was then in the correct place before the testing began.

Overall, 125 individual runs were planned over the 5 days of testing, each run being 2 minutes long and allowing 1 minute between each test for the current to stabilise.

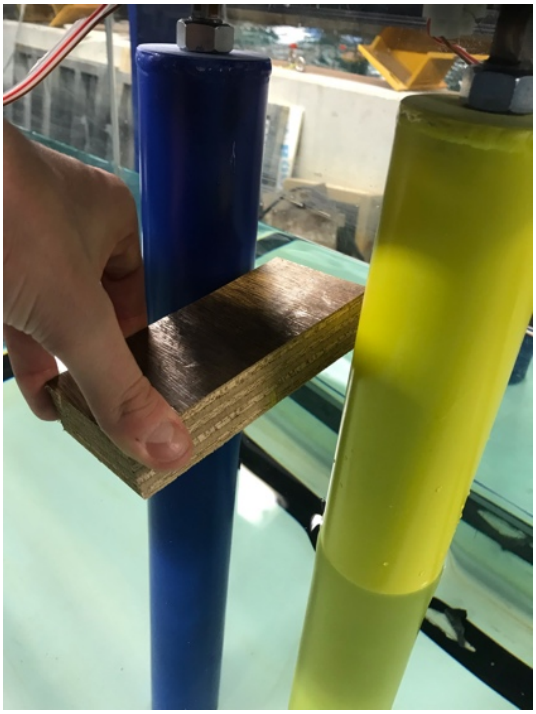

Figure 14: Measuring the gap between the piles.

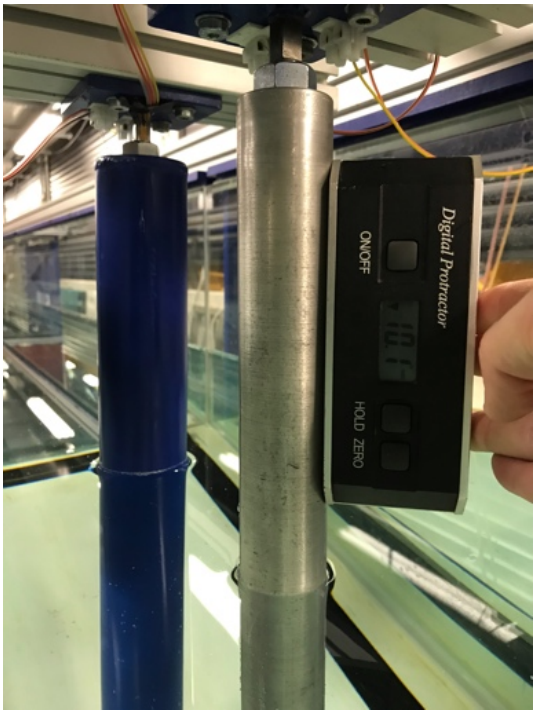

Figure 15: Measuring the angle of the piles using a digital protractor.

Results

Cross-Flow Oscillations and Vortex Shedding

Reynolds Number, Strouhal Number and Vortex Shedding Frequency
Using **equations *(2)*, *(3)*** and ***(4)*** discussed in section 0, the Reynolds numbers, Strouhal numbers and the vortex shedding frequency can be calculated for each combination of current velocity and pile diameter. The kinematic viscosity of water has been taken as 1.31×10^{-6} m^2/s, assuming it is at 10°C (Engineers Edge, 2019). The period of the oscillations has been calculated by $1 \div$ vortex shedding frequency.

Table 3: Reynolds number, Strouhal number and vortex shedding frequency of each current velocity and pile diameter.

	Current Velocity (m/s)				
	0.1	0.3	0.5	0.7	0.9
Pile Diameter (mm)	**Pile Reynolds Number**				
64	4897	14690	24484	34277	44070
40	3060	9181	15302	21423	27544
30	2295	6886	11477	16067	20658
	Strouhal Number				
64	0.197	0.198	0.198	0.198	0.198

40	0.197	0.198	0.198	0.198	0.198
30	0.196	0.197	0.198	0.198	0.198
	Vortex Shedding Frequency (Hz)				
64	0.308	0.927	1.546	2.164	2.783
40	0.492	1.482	2.472	3.462	4.452
30	0.654	1.974	3.294	4.614	5.934
	Oscillation Period (s)				
64	3.245	1.079	0.647	0.462	0.359
40	2.033	0.675	0.405	0.289	0.225
30	1.528	0.506	0.304	0.217	0.169

Each of the runs specified in the run matrix were run for 2 minutes. Initially, 5 runs with a single 64 mm pile were conducted for all 5 current velocities. **Figure 16** presents 20 seconds of the results from the middle of the test of the cross-flow oscillations from the 5 initial runs, run ID's 0.0 to 0.4. The cross-flow data has been taken from the strain gauges attached to the side of the pile. Therefore, the movements recorded are of the pile in a direction perpendicular to the flow.

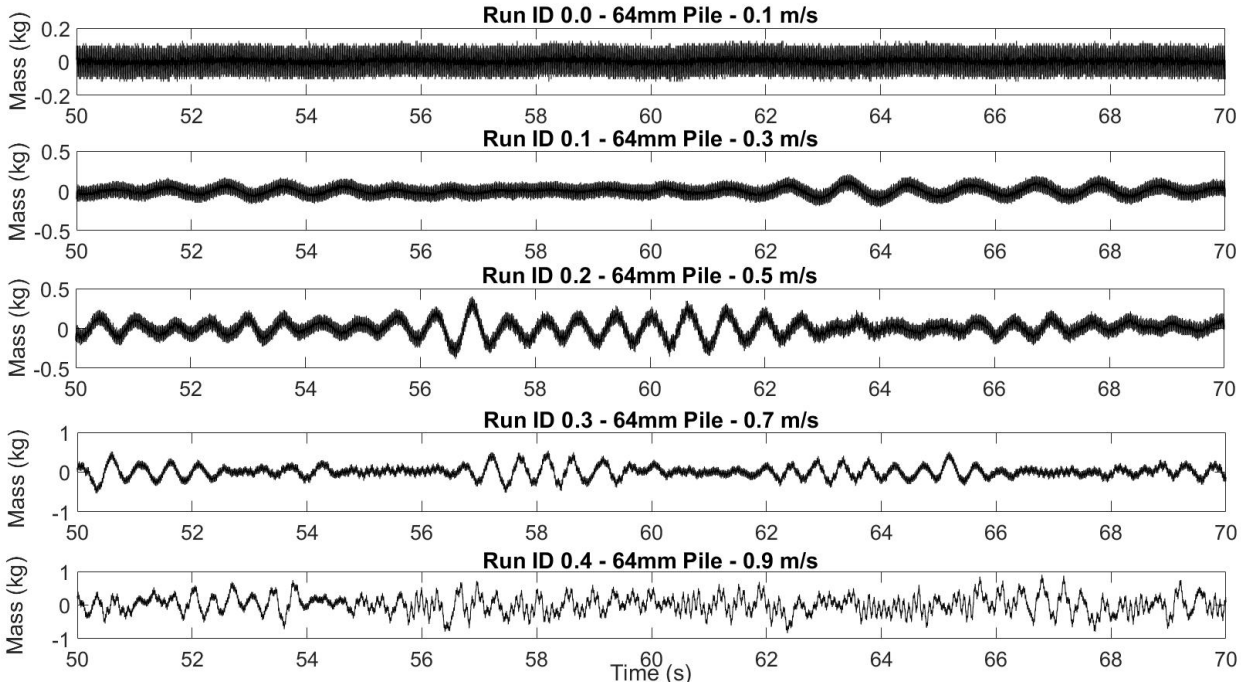

Figure 16: Raw data results from tests 0.0 - 0.4.

Figure 16 shows a clear increase in oscillation amplitude with an increase in current velocity. Although, it's not yet clear how the frequency of the oscillations is affected by the velocity of the current.
The plots show that during 0.1 m/s experiment there was very little oscillation in the cross-flow direction. **Figure 17** displays the results from the 0.1 m/s tests for all 3

individual piles. The results show that all 3 diameters of pile experience little to no oscillation when the current was set to 0.1 m/s. The data that is displayed is produced by the noise from the strain gauges. Therefore, none of the 0.1 m/s tests will be analysed any further for crossflow oscillations. This is due to the vortex shedding frequency being too low and hence the period of the oscillation being too high for the system to be able to record it.

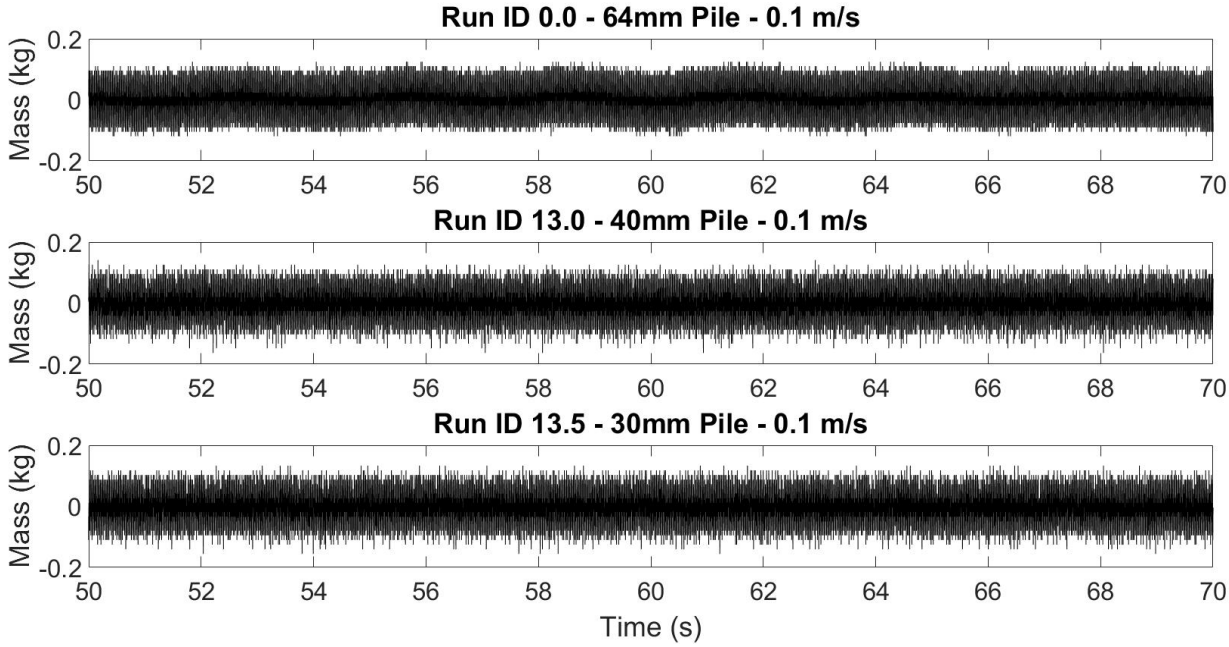

Figure 17: Raw data results from tests 0.0, 13.0 and 13.5.

Spectral analysis of the loading time series was used to identify the frequency of forcing of the piles. Spectral analysis was carried out using MATLAB, following the approach of Oppenheim and Schafer (1975). Velocity time spectra of the in-line and cross-flow loading time series were calculated using a time series of length 131072 points, divided into 8 non-overlapping sections of length 16384 points, and 7 overlapping sections, with 50% overlap. Sections were Hanning windowed and Fast Fourier Transformed to give 8192 energy estimates between 0 and the Nyquist frequency, with a resolution of 1.24×10^{-3} Hz. **Figure 18** presents the frequency spectrum for run ID's 0.1, 13.1 and 13.6. All 3 individual piles with a current velocity of 0.3 m/s.

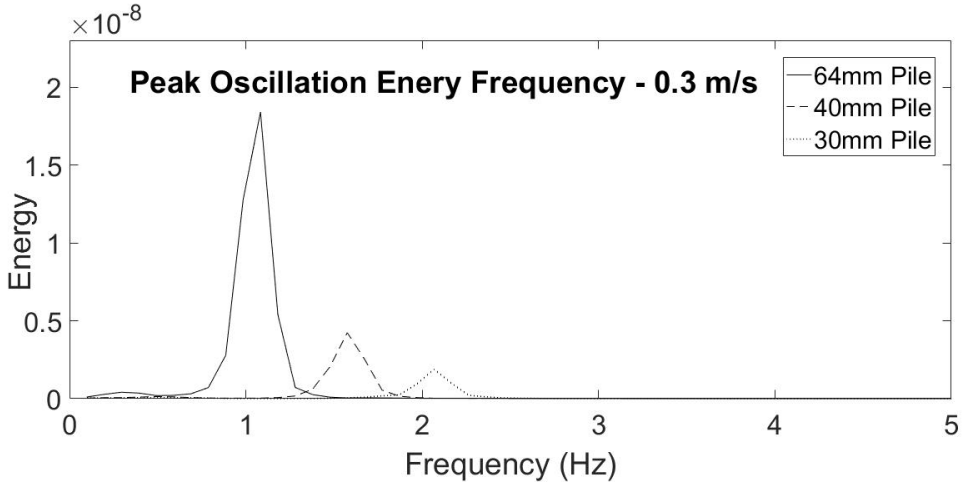

Figure 18: Frequency spectrum of run ID's 0.1, 13.1 and 13.6.

The spectrum shows 3 peaks in the data corresponding to the frequencies of the oscillations of the 3 different pile diameters. The frequencies occur at approximately 1.1 Hz, 1.6 Hz and 2.1 Hz for the 64 mm, 40 mm and 30 mm pile respectively. **Figure 19** presents the same spectrum as in **Figure 18** but shows a much larger range of frequencies. The graph shows peaks in the data around 0 Hz, which coincide with the peaks shown in **Figure 18**. Spikes decreasing in height can also be seen in the data every 100 Hz from 50 Hz onwards. i.e. at 50 Hz, 150 Hz, 250 Hz 350 Hz etc. This is most likely caused by an electronic error in the strain gauge and recording equipment since the spikes are at regular intervals. It is possible to filter out the errors, however this has not been done as the errors only begin to occur at 50 Hz and do not affect the data this report is concerned with.

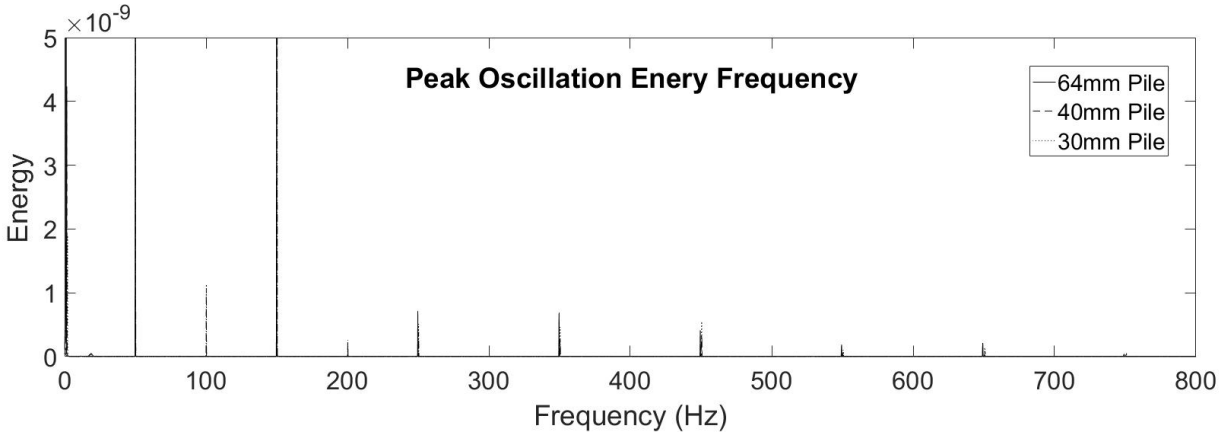

Figure 19: Figure 18 showing a larger frequency range with spikes in the data every 100 Hz.

Figure 20 presents the measured frequencies from **Figure 18**, along with the theoretical frequencies of each pile with a current velocity of 0.3 m/s as calculated in **Table 3**.

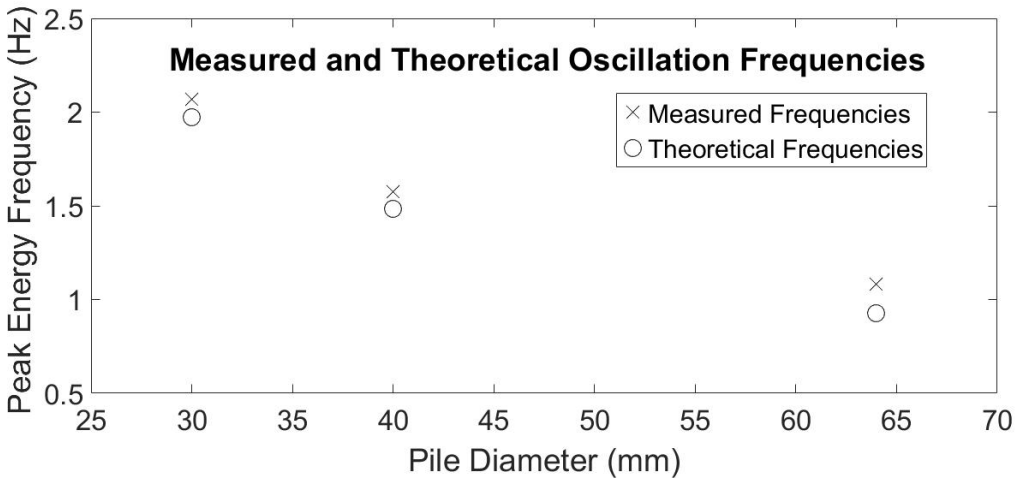

Figure 20: Measured frequencies against theoretical frequencies with a current velocity of 0.3 m/s.

As shown, the measured frequencies are very close to the calculated theoretical frequencies. For all 3 piles, the measured frequencies are more, however the differences are very small. The frequency increase from the theoretical value for the 64 mm, 40 mm and 30 mm diameter piles are 16.83%, 6.28% and 4.71% respectively. **Table 4** presents the measured frequencies, theoretical frequencies and percentage differences of the 12 runs with individual piles and current velocities 0.3, 0.5, 0.7 and 0.9 m/s.

Table 4: Measured and Theoretical Frequencies for all single piles at all current velocities.

Pile Diameter (mm)	Measured / Theoretical Frequency (Hz)	Current Velocity (m/s)			
		0.3	0.5	0.7	0.9
64	Measured Frequency	1.083	1.674	2.264	2.855
	Theoretical Frequency	0.927	1.546	2.164	2.783
	Percentage Difference	16.83%	8.28%	4.62%	2.59%
40	Measured Frequency	1.575	2.560	3.347	4.233
	Theoretical Frequency	1.482	2.474	3.462	4.452
	Percentage Difference	6.28%	3.48%	3.32%	4.92%
30	Measured Frequency	2.067	3.347	3.938	4.922
	Theoretical Frequency	1.974	3.294	4.614	5.934
	Percentage Difference	4.71%	1.61%	14.65%	17.05%

Table 4 shows how in most cases the measured and theoretical frequencies are very close to each other. But, a couple of the results have percentage errors of greater than 14%, especially the 30 mm pile during the 0.7 m/s and 0.9 m/s tests.
Figure 21 displays the energy spectrum from run ID's 0.3, 13.3 and 13.8 which correspond to the tests of all the individual piles with a flow velocity of 0.7 m/s. Although the predominant oscillation frequency occurs at approximately 3.9 Hz, **Table 4** shows that this is 14.65% different to the theoretical frequency. Another

spike in the data, shown on **Figure 21**, occurs at 14.85 Hz, meaning that the 30 mm pile was experiencing more than 1 frequency of oscillation.

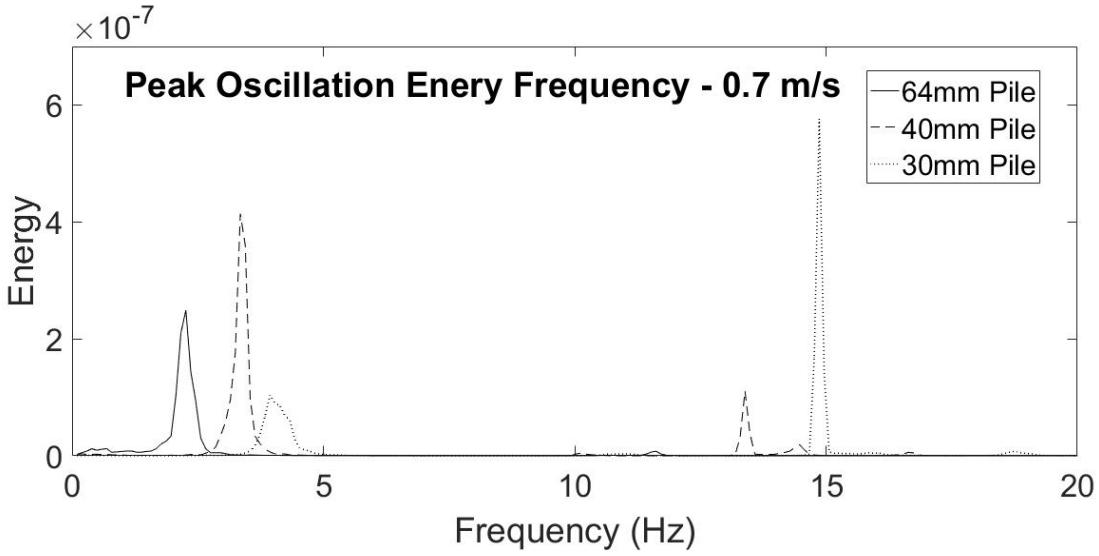

Figure 21: Frequency spectrum of run ID's 0.3, 13.3 and 13.8.

Figure 22 displays the energy spectrum from run ID's 0.4, 13.4 and 13.9, which correspond to the tests of all the individual piles with a flow velocity of 0.9 m/s. The same spike at approximately 14.85 Hz can be seen, accounting for the error between the measured and theoretical frequencies. As the higher frequency spikes occur at approximately the same frequency on both tests, this indicates that the higher flow velocities are inducing a vibration in the system with a frequency of approximately 14.85 Hz.

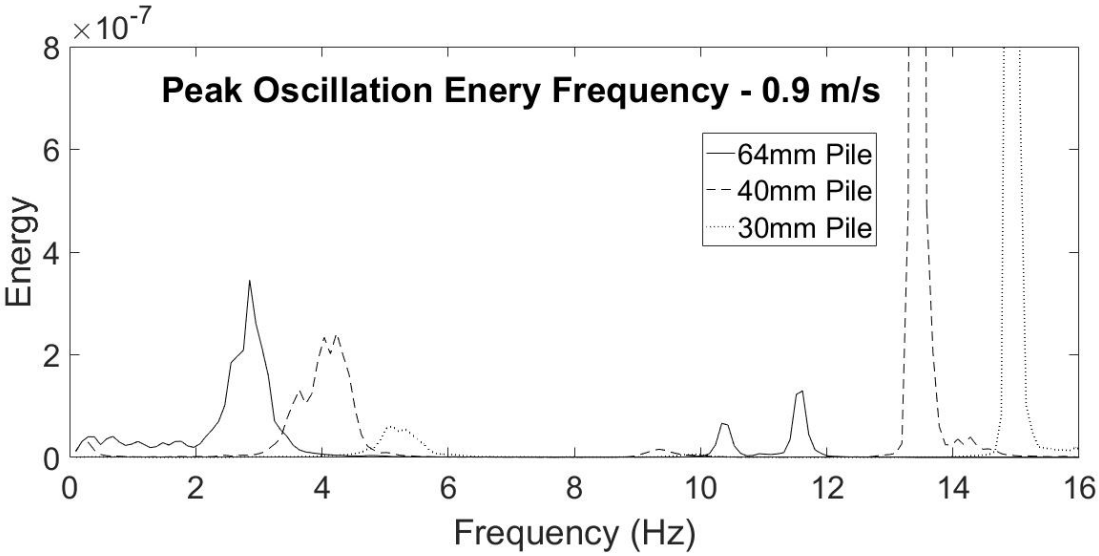

Figure 22: Frequency spectrum of run ID's 0.4, 13.4 and 13.9.

Effects of Spacing on Oscillation Frequency

Figure 23 presents the frequency of the cross-flow oscillations of a 64 mm downstream pile, where the upstream pile is also 64 mm. The results show the oscillations for flow velocities of 0.3, 0.5, 0.7 and 0.9 m/s with centre to centre

spacings of 3 - 10 diameters. Where the results given at '0 diameters' are the oscillation frequencies of the upstream 64 mm pile and the horizontal lines are the calculated theoretical frequencies for each flow velocity, taken from **Table 3**.

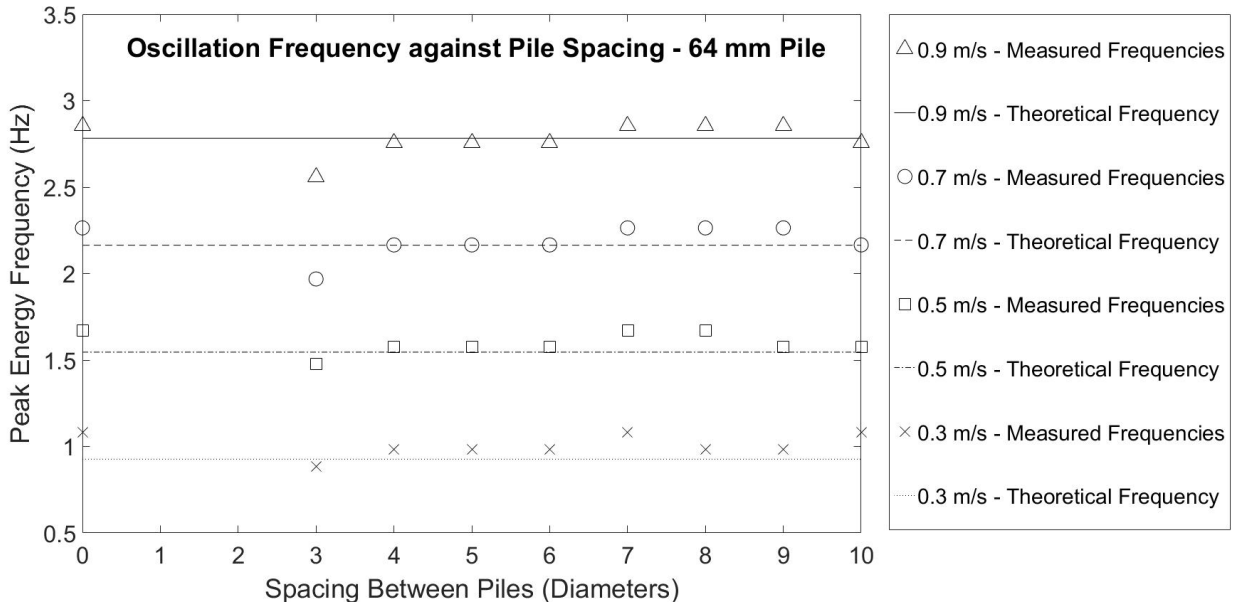

Figure 23: 64 mm pile oscillation frequency against distance between piles for all current velocities.

A general pattern can be seen throughout the results:

- As expected, the frequency of the oscillations increases with flow velocity.
- It's already been established that the frequency of the oscillations of the upstream pile is slightly more than the theoretical frequency calculated.
- At all current velocities, 3 diameters away the oscillation frequency is less than the theoretical, especially for the higher current velocities.
- At 4, 5 and 6 diameters, at all current velocities, the frequency is almost identical to the theoretical.
- At 7, 8 and 9 diameters, at all current velocities, the frequency is slightly more than the theoretical, similar to what is experienced by the upstream pile.
- Finally, 10 diameters away the frequency of the oscillations almost matches the theoretical once again, except at 0.3 m/s where is it greater than the theoretical.

As explained in 0, when the pile diameter was changed, the upstream pile remained at 64 mm to reproduce situations like at the Thanckes Jetty, where a variety of larger and smaller diameter piles have been used close to each other. **Figure 24** presents the frequency of the oscillations of the downstream 40 mm pile for all current velocities and spacings, with the size of the upstream pile remaining at 64 mm.

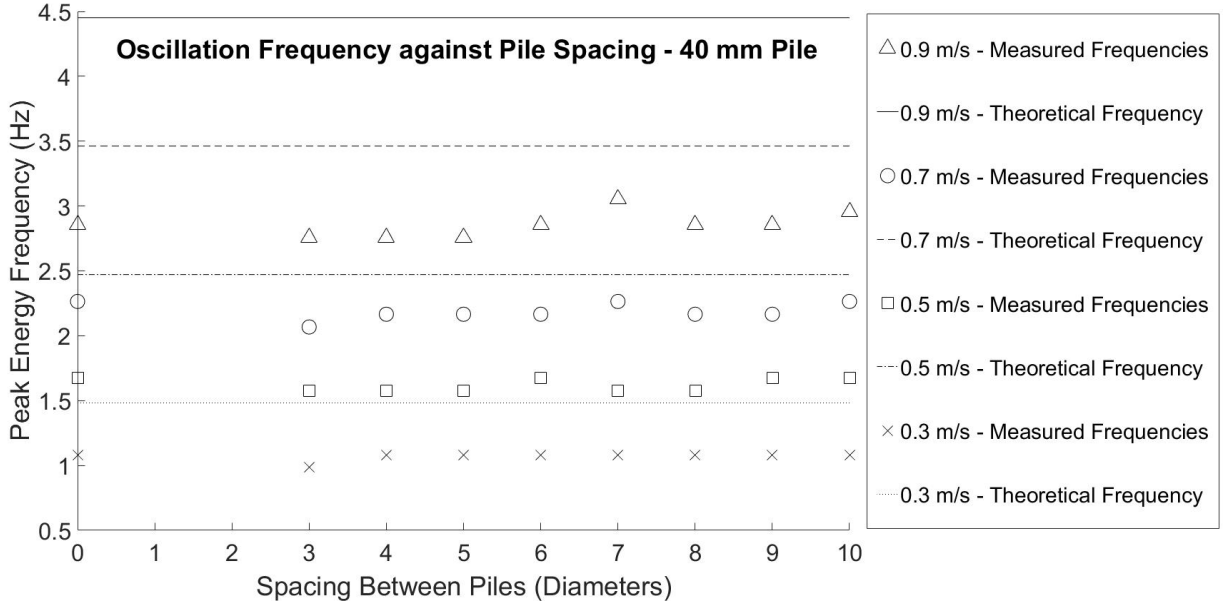

Figure 24: 40 mm pile oscillation frequency against distance between piles for all current velocities.

The result at '0 diameters' remains the frequency of the oscillations of the upstream 64 mm pile. The graph shows how the frequency of the oscillations at all locations and for all current velocities is significantly less than the theoretical, but very similar to the oscillations of the 64 mm pile. Additionally, the higher the velocity of the current flow, the more the frequencies measured are less than their corresponding theoretical frequencies. A general slight increase in frequency can be seen from 3 to 7 diameters in spacing, it then reduces at 8 diameters and remains roughly constant until 10 diameters away. Figure 25 presents the results for a downstream 30 mm pile where the upstream pile remained at 64 mm.

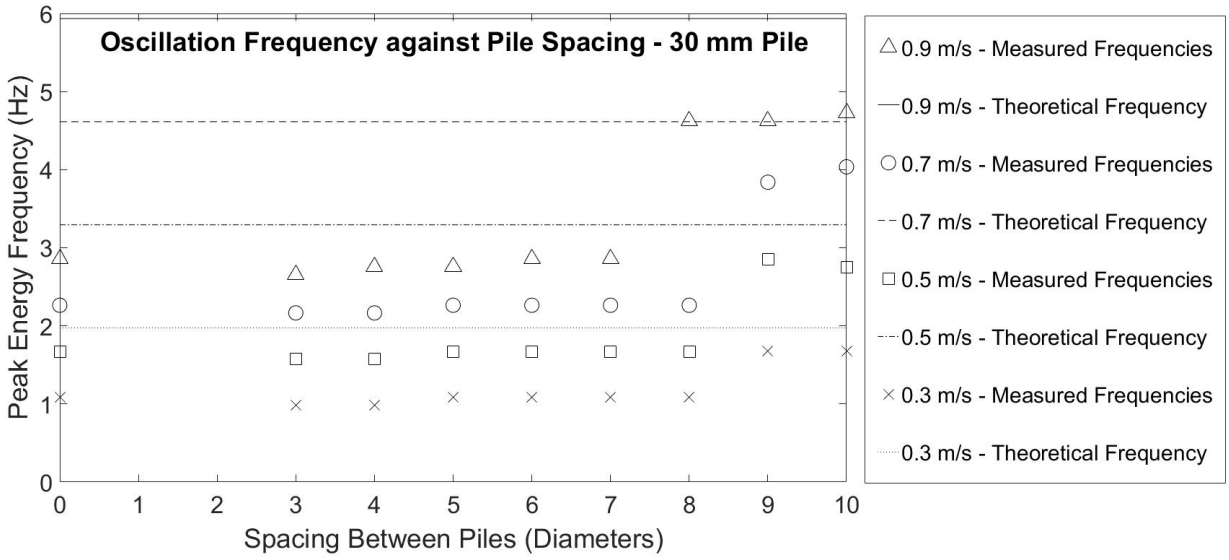

Figure 25: 30 mm pile oscillation frequency against distance between piles for all current velocities.

The results presented in **Figure 25** show that the frequencies of the oscillations experienced by the 30 mm pile are roughly the same as the oscillations experienced

by the 40 mm and 64 mm piles. Except for when the spacing was 8, 9 and 10 diameters. At a spacing of 8 diameters, the results at a current velocity of 0.1, 0.3 and 0.5 m/s follow the same general pattern as the rest of the results. However, at 0.9 m/s the frequency of the oscillations experienced by the pile were much higher than expected based on the other results. The frequencies are still lower than the theoretical value but almost match the frequency experienced by the single 30 mm pile. This is the same for 0.9 m/s at 9 and 10 diameters spacing. Additionally, the results for 0.3, 0.5 and 0.7 m/s at 8 and 9 diameters spacing do not follow the trend in the results, although they still do not match the theoretical frequency. These results show that the influence of the upstream pile on the oscillations of the downstream start to reduce when the spacing reaches 8 to 10 diameters. However, this was not seen with the 64 mm and 40 mm pile.

In summary, the results for the 64 mm pile are as expected. The frequency of the cross-flow oscillations is very close to the theoretical but does change slightly when the downstream pile is close to the upstream pile and therefore in the wake of its vortices. But the frequency does return to the theoretical further downstream when the pile is experiencing steady flow once again. The results for the 40 mm and 30 mm pile show that the frequency of their oscillations is mainly governed by the frequency of the oscillations of the larger upstream pile, as their oscillation frequency is extremely different to the oscillations of a single pile of the same diameter on its own. Therefore, the upstream pile must be impacting the movements of the smaller downstream piles.

Steady Drag Force

As discussed, the steady drag force on a submerged object can be presented by the following equation (BSI, 2016):

$$F_D = \frac{1}{2}(C_D \rho u^2 A_n) \quad \textit{(5)}$$

The Reynolds numbers for the experiment have been calculated in **Table 3** and range from 2295 to 44070. The value of the drag coefficient, C_D for circular cylinders varies with relative surface roughness's, k/D. However, for Reynolds numbers less than 10^5, C_D tends to 1.2, for all values of k/D. Therefore, a drag coefficient of 1.2 has been used throughout the calculations. **Table 5** presents the theoretical steady drag forces on the singular 64 mm, 40 mm and 30 mm piles for all current velocities using **equation *(1)*.**

Table 5: Theoretical steady drag forces for all singular piles at all current velocities.

	Current Velocity (m/s)				
	0.1	0.3	0.5	0.7	0.9
Pile Diameter (mm)	**Theoretical Steady Drag Force, F_D (kg)**				
64	0.020	0.176	0.489	0.959	1.585
40	0.012	0.110	0.306	0.599	0.991
30	0.009	0.083	0.229	0.450	0.743

As well as the cross flow oscillations, the strain gauges were also recording the pile movements in an in-line direction, parallel to the flow. The steady drag forces have been calculated by converting the voltage measured by the strain gauges and transforming it to a force using the calibration equations calculated in 0. The mean value of the in-line force has been calculated to avoid measuring the maximum voltage an any anomalous spikes within the data.

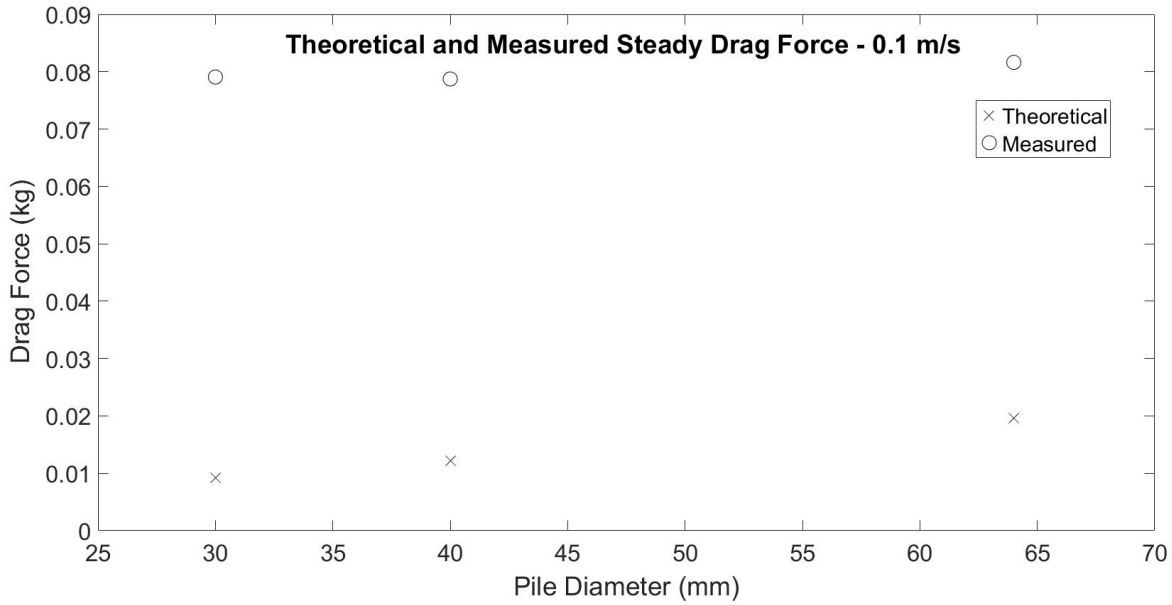

Figure 26: Theoretical and measured steady drag forces at a current velocity of 0.1 m/s.

Figure 26 compares both the theoretical and measured steady drag forces on all 3 piles with a current velocity of 0.1 m/s. As shown, the measured values are much larger than the theoretical and appear to all have roughly the same value for all 3 piles. Upon further analysis of the recorded data it has been conculded that, similarly to section 0, the data recorded is just the noise produced from the strain gauges and that the flow velocity is too slow for any in-line forces to be recognised. **Figure 27** presents the raw data from the 0.1 m/s tests on all 3 individual piles, it shows how the signal produced by the strain gauges remains the same for all tests and has an amplitude of approximately 0.1 kg. This matches with the measured forces of 0.08 kg displayed on **Figure 26**.

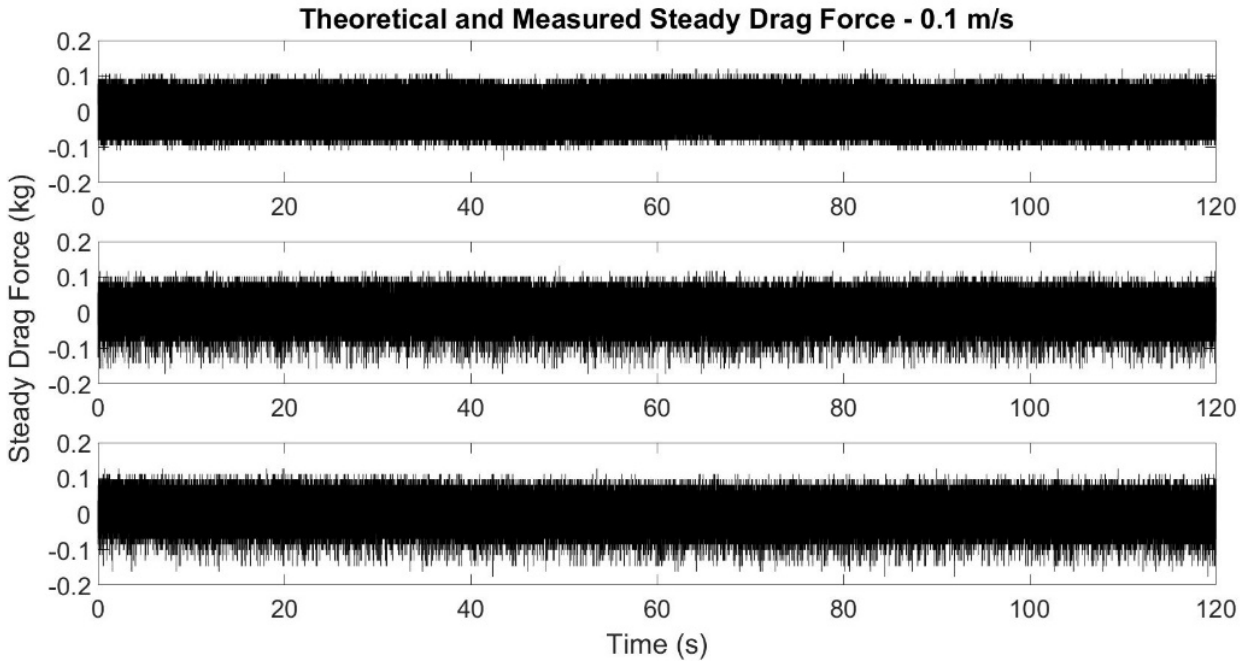

Figure 27: Raw data from the 0.1 m/s experiments on all 3 piles.

Table 6 presents all the measured steady drag forces for all piles at all current velocities. It shows that all the data from the 0.3 m/s experiments also result in steady drag forces of approximately 0.08

Table 6: Measured steady drag forces for all singular piles at all current velocities.

	Current Velocity (m/s)				
	0.1	0.3	0.5	0.7	0.9
Pile Diameter (mm)	**Measured Steady Drag Force, F_D (kg)**				
64	0.082	0.085	0.109	0.188	0.455
40	0.079	0.080	0.092	1.080	3.339
30	0.079	0.079	0.088	2.143	3.687

The in-line steady drag results show how the forces increase with current velocity in all cases, espcially when the velocity becomes much greater. Which is expected as the drag force is proportional to the flow velocity squared, as shown in **equation *(1)***. However, the steady drag forces measured at 0.5 m/s, 0.7 m/s and 0.9 m/s also appear to show a large discrepancy between the theoretical and measured drag force valules. Especially during the 0.7 m/s and 0.9 m/s cases, as the forces measured by the strain gauges on the 30 mm and 40 mm pile are greater than the forces on the larger 64 mm pile. This has been caused by how the piles were acting in the higher current flows. Rather than a steady force being applied to the pile, resulting in a constant force being measured by the strain gauges, the high flow velocity caused the piles to rapidly shake in an in-line direction. Ignoring the errors

that have been introduced at the higher current velocities, the results do show an increase in force with an increase in pile diameter for the same flow velocity, as is to be expected with the steady drag force equation, except for the 0.7 m/s and 0.9 m/s cases.

Figure 28 to **Figure 32** display the theoretical steady drag forces calculated in **Table 5** along with the measured in-line forces on each pile at all 5 current velocities.

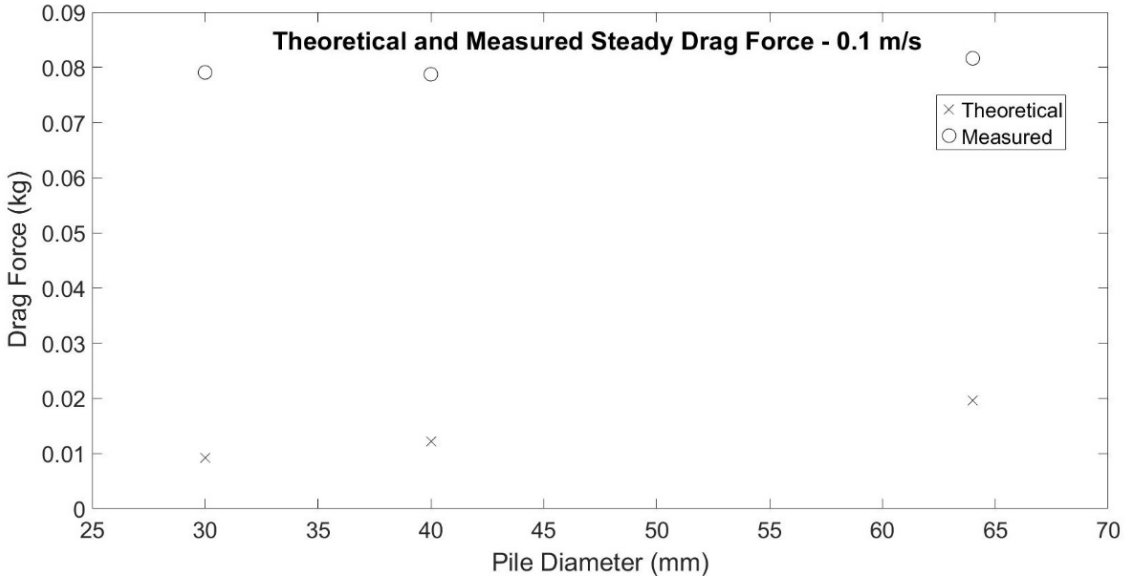

Figure 28: Theoretical and measured in-line steady drag forces at 0.1 m/s.

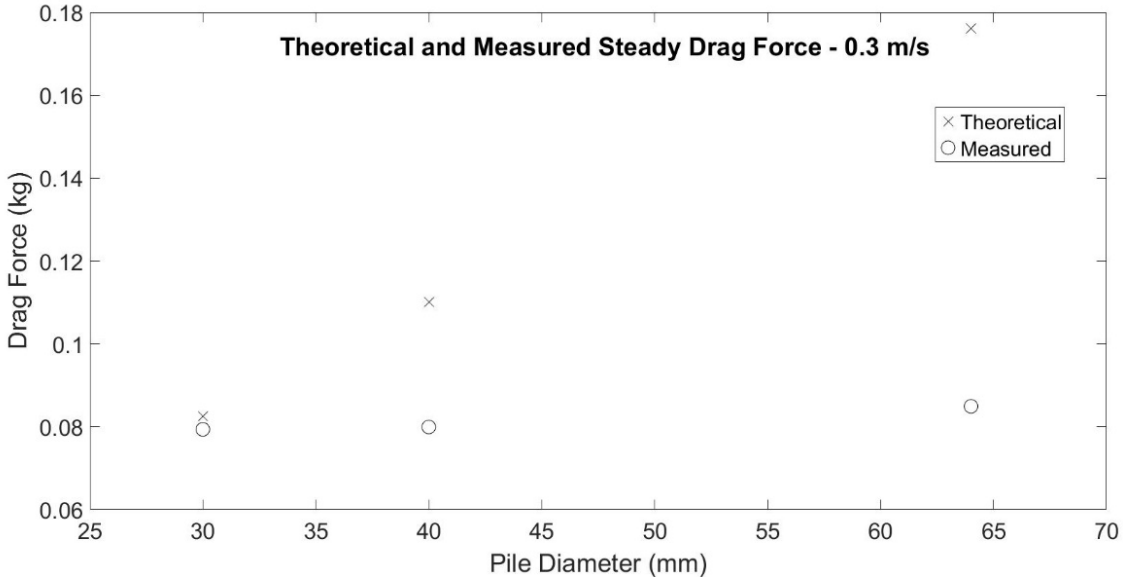

Figure 29: Theoretical and measured in-line steady drag forces at 0.3 m/s.

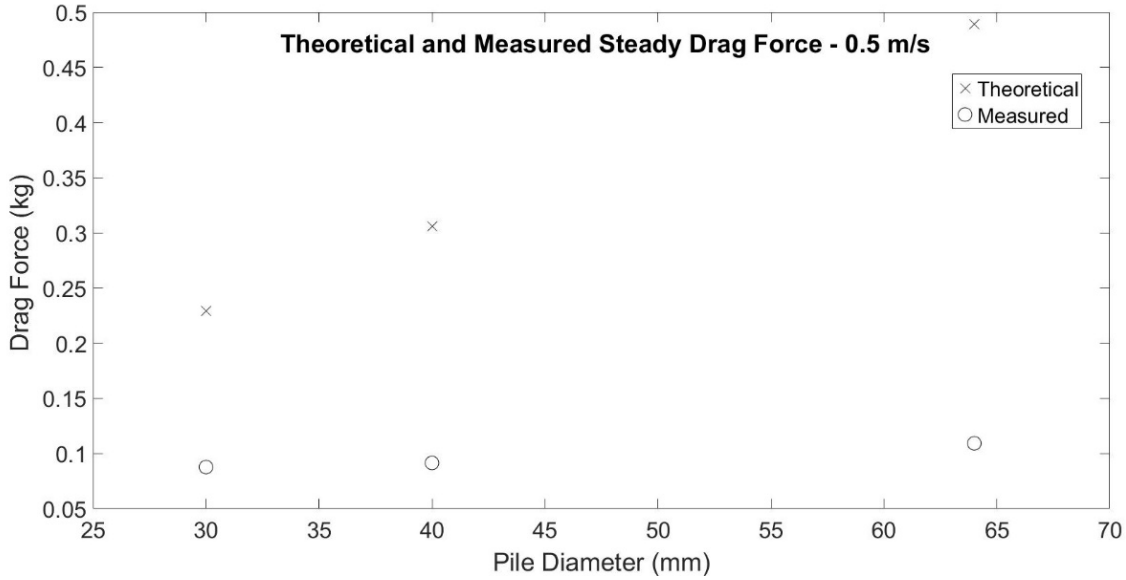

Figure 30: Theoretical and measured in-line steady drag forces at 0.5 m/s.

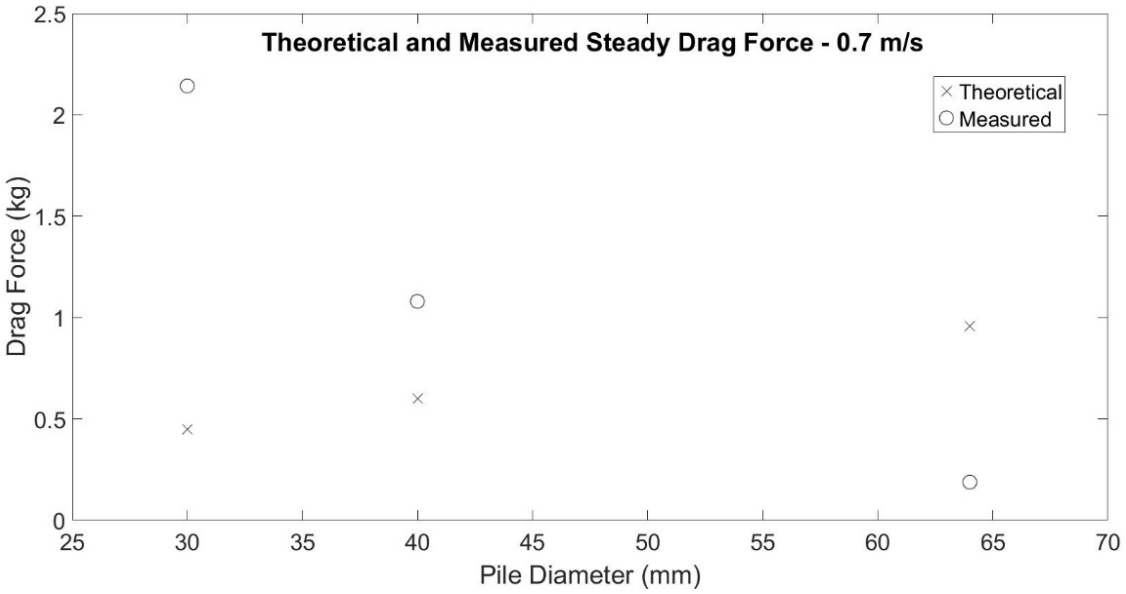

Figure 31: Theoretical and measured in-line steady drag forces at 0.7 m/s.

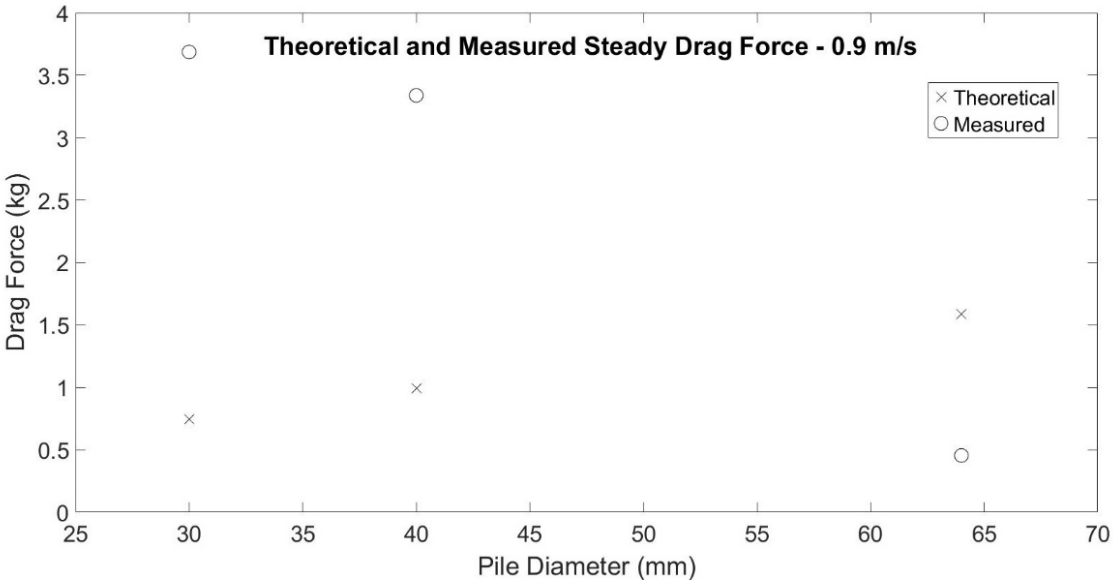

Figure 32: Theoretical and measured in-line steady drag forces at 0.9 m/s.

Despite the errors at the lower and higher velocities the plots give a good indication of how much of an effect a resonating system can have on the forces experienced by a cantilevered pile. Emphasising the importance of ensuring resonance does not occur during construction.

Effects of Spacing on Steady Drag Force

Since the slower and faster of the flow velocities tested did not produce valid results, the 0.5 m/s tests have been used to analyse how the spacing between the pile affects the steady drag force experienced by the downstream pile.

Figure 33 shows the variation of measured steady drag force with distance from the upstream pile. The graph shows the steady drag force experienced by the 64 mm pile downstream of another 64 mm pile. **Figure 34** and **Figure 35** present the same data but for a downstream 40 mm and 30 mm pile respectively, with the upstream pile remaining at 64 mm.

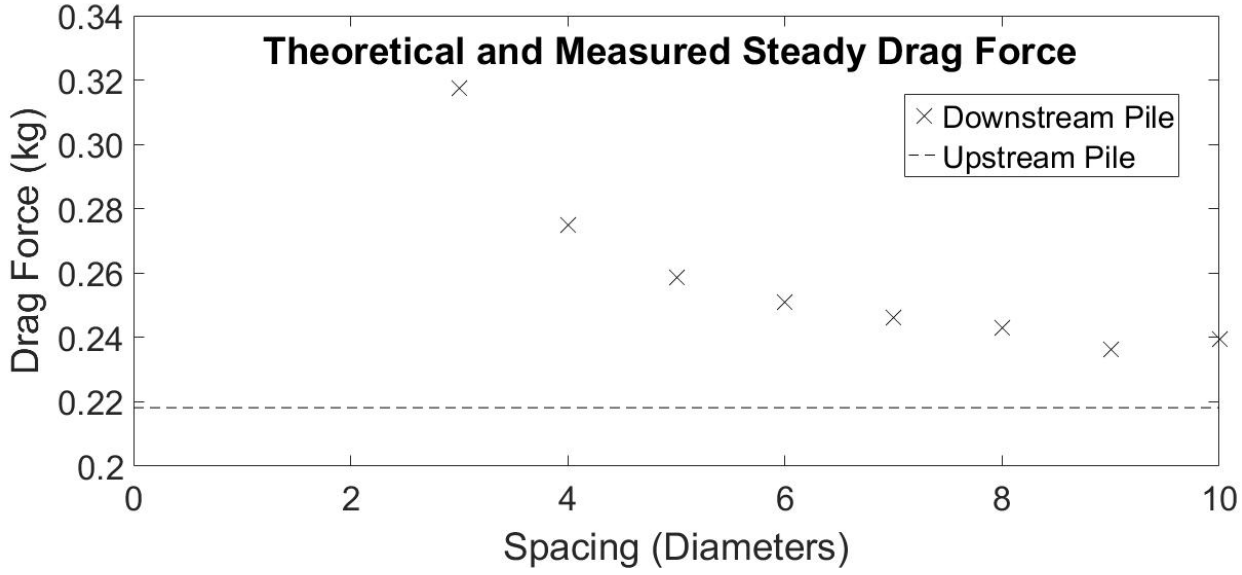

Figure 33: Measured steady drag forces on a 64 mm pile for all spacings at 0.5 m/s.

As shown in **Figure 33**, the steady drag force on the downstream pile 3 diameters away is significantly more than what is experienced by the upstream pile. The force then decreases with distance away from the pile until it appears to stabilise at approximately 0.24 kg, slightly more than the force experienced by the upstream pile.

Figure 34 and **Figure 35** both show a similar pattern. The steady drag force is greater than the force on the upstream pile 3 diameters away. Then, the force steadily decreases as the spacing between the 2 piles increases. Likewise, the force then appears to become more stable around a spacing of 9 to 10 diameters. However, opposite to the 64 mm pile, the drag force on the 40 mm and 30 mm piles drops below the force experienced by the upstream pile. On both occasions, the force becomes less than on the upstream pile between a spacing of 4 and 5 diameters.

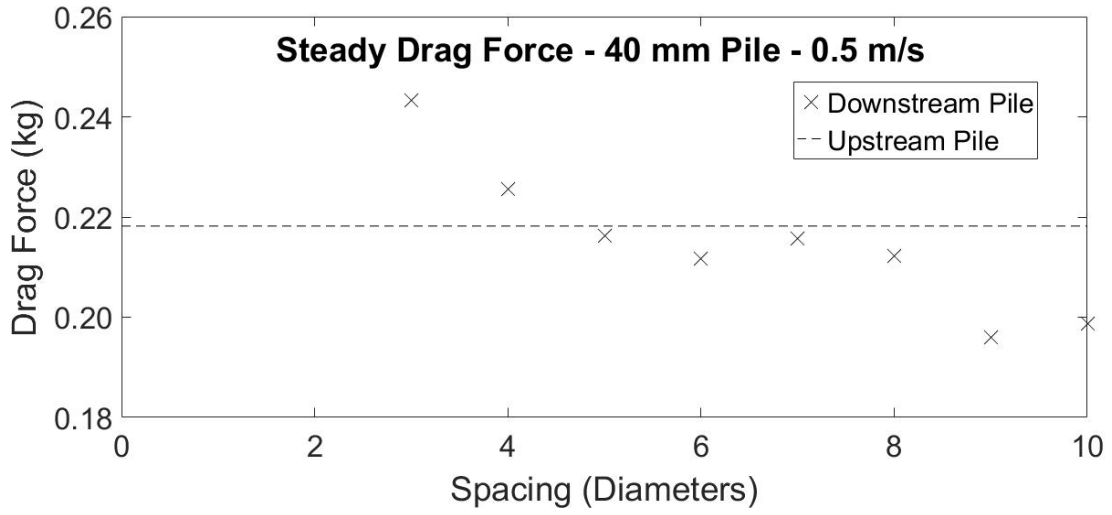

Figure 34: Measured steady drag forces on a 40 mm pile for all spacings at 0.5 m/s.

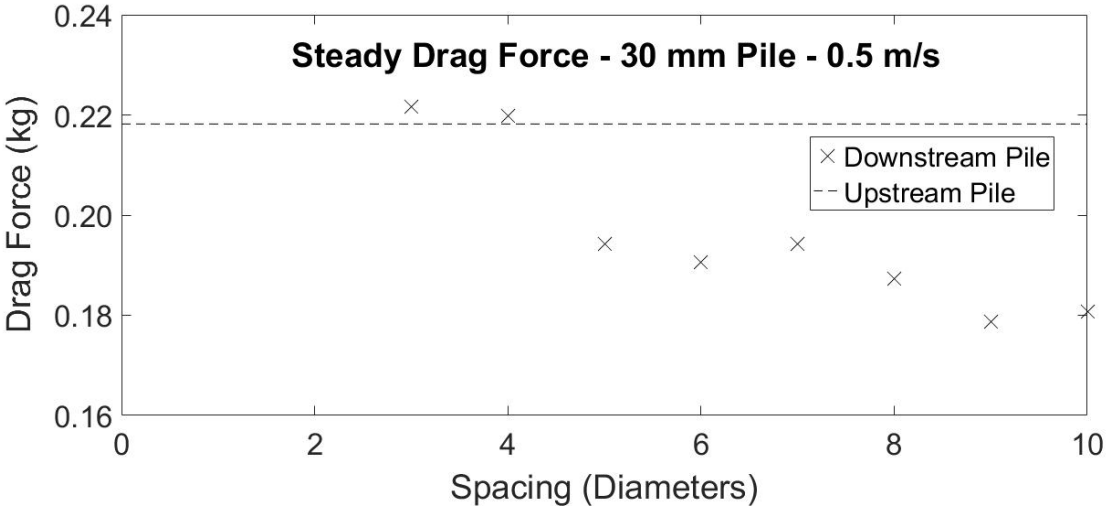

Figure 35: Measured steady drag forces on a 30 mm pile for all spacings at 0.5 m/s.

Discussion

Relevance

The results presented provide valuable insight into the original research objective, to discover how a pair of in-line piles behave in terms of cross-flow oscillations and in-line steady drag force when placed in a current flow. Similar experiments have been conducted by various authors over the past few decades, some with comparable conditions and results and some without. Many aspects of the investigation carried out by Miles et al (2017), looking into current and wave effects around monopiles, used similar conditions. Miles used current conditions ranging from 0.75 to 1.75 m/s, which were representative of several UK and Ireland windfarm locations. This experiment used conditions based on the slower velocities of approximately 0.7 m/s at the Thanckes river Tamar site and the faster current conditions of up to 2.5 m/s at the mouth of the river Humber, the location of the Immingham Oil Terminal pile failures. Although this investigation used slightly more unrealistic velocities of up to 4.5 m/s to explore any trends, the lower speeds were realistic of real locations around the UK. The depth of 0.5 m used was based on the depths at the Thanckes site with a 1:25 scale ratio. Miles also used a depth of 0.5 m which was based on various sites around the UK, like his current conditions. Similar to this study, Miles identified oscillations in the current downstream of the pile that matched the eddy shedding frequency calculated from the Strouhal number for the conditions.

Miles' findings showed that flow conditions downstream of the monopile returned to within 5% of the steady state conditions roughly 8.7 diameters downstream. Although this report did not investigate the current conditions downstream, the steady drag forces on the piles give a good representation of how the current conditions vary with distance from the upstream pile. **Figure 33**, **Figure 34** and **Figure 35** show how the steady drag force on the downstream pile decreases with spacing and that it appears to level out around 9 to 10 diameters away, for all 3 diameters of pile used, with the upstream pile remaining at 64 mm. This shows that the flow conditions become more regular 9 to 10 diameters away, similar to what Miles discovered, despite the large difference in pile diameter used, 64 mm rather than 200 mm.

Although the investigation conducted by Mittal and Kumar (2001) was computational rather than practical, this experiment also shared some similarities. Mittal and Kumar used a cylinder spacing of 5.5 diameters, within the range used during this investigation. Okla et al (1972) and Xu and Zhou (2004) also carried out similar experiments on tandem piles and demonstrated that vortex shedding that affected the downstream pile occurred between 3 and 5 diameters downstream. Xu and Zhou discovered that the critical spacing where vortex co-shedding started to occur was between 3 and 5 diameters, but because spacings of 1 and 2 diameters were not able to be measured it is difficult to determine if there was any change in the oscillations from a 1 to 3 diameter spacing.

Limitations

One of the main limitations of the experiment was the way the MiniTec was arranged to support the piles above the flume tank. Initial testing showed that the whole rig, not just the piles, was susceptible to shaking when the higher flow velocities were used. This meant that the results did not give a true representation of how the piles

were reacting. Therefore, the MiniTec was rearranged with the aim of reducing the shaking. Unfortunately, this stopped the smaller spacings of 1 and 2 diameters from being able to be tested, as the piles could not be placed close to each other because of the MiniTec bars. Although it would have been useful to measure the oscillations and forces much closer to the upstream pile, the main vortex shedding effects occurred between 3 and 5 diameters in similar experiments. Spacings that were investigated in this test ranged from 3 to 10 diameters, centre to centre. Xu and Zhou's investigations ranged from 1 to 15 diameters, centre to centre.

Another issue that was identified in section 0 was the large amount of background noise picked up by the strain gauges and that in the slow flow velocity cases, the noise produced was larger than the steady drag or oscillations forces. This was due to the sensitivity of the gauges and the high sampling frequency. To stop this, a lower sampling rate could have been used, but that would reduce the accuracy of the results. In the experiment conducted by Xu and Zhou, a sampling rate of 3500 Hz was used, showing that using a high sampling rate is acceptable, although this was used for measuring the velocity of air with 2 hot wires. A larger diameter pile could have reduced the effect of the noise generated by the gauges as the drag force experienced would have been greater. However, even a pile of double the size i.e. 128 mm diameter would experience a theoretical steady drag force of only 0.04 kg with a flow velocity of 0.1 m/s and the magnitude of the noise emitted by the gauges was approximately equal to 0.08 kg. The errors were reduced for the oscillating loads as the frequency of the oscillations were larger compared to the frequency of the noise. Therefore, the loading was identifiable in the spectral analysis.
When the experiment was completed and the piles were being removed it was noticed that the 30 mm pile was filled with water, when it should have been empty. Initially, it was thought that this could affect the results. But, the pile was temporarily repaired and the 5 tests with the individual pile were re-run. **Figure 36** presents the frequency of the cross-flow oscillations from the 0.3 m/s single pile runs (run ID's 13.6 and 14.1) before and after the pile was repaired. It clearly shows that the frequency was the same on both occasions and therefore the results from all the other tests have not been affected.

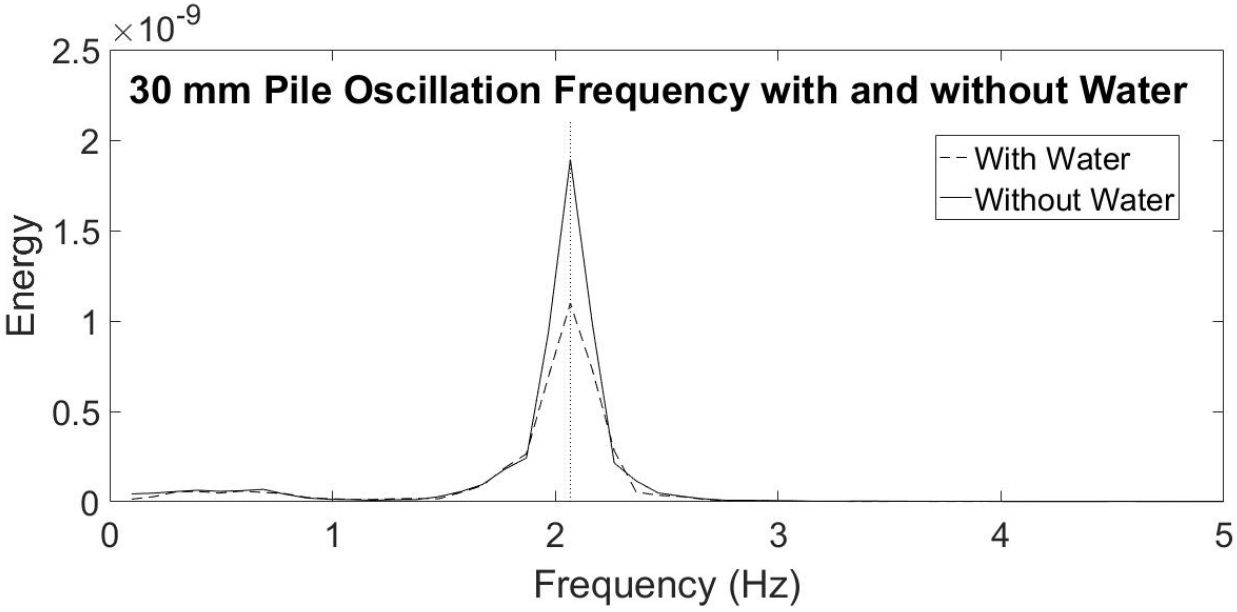

Figure 36: Frequency of oscillations of 30 mm pile with and without being filled with water.

Effects to the Design of Piles

The results from the experiment could have an impact on the way piles are designed. A common approach in industry is to identify the natural frequency of the member using **equation *(6)*** *(Tomlinson, 2007)*, then calculate the critical velocity using **equation *(7)*** (BSI, 2016) and ensure that the flow conditions at the site do not exceed the critical velocity.

$$f_N = \frac{K'}{L^2}\sqrt{\frac{EI}{M}} \qquad \textit{(6)}$$

Where;

- f_N is the natural frequency of the member, in Hertz (Hz);
- K' is a dimensionless constant that depends of the end restraint;
  - 0.56 for cantilevered;
  - 2.45 for propped;
  - 3.56 for fully fixed;
- L is the length of the member, in metres (m);
- E is the elastic modulus of the member, in Newtons per square metre (N/m^2);
  - 2.1×10^{11} N/m^2 for structural steel;
- I is the moment of inertia, in metres to the power 4 (m^4);
- M is the effective mass per unit length of the pile, in kilograms per metre (kg/m).

$$V_{crit} = K f_N W_S \qquad \textit{(7)}$$

Where;

V_{crit} is the critical flow velocity, in metres per second (m/s);
K is a dimensionless constant equal to:
- 1.2 for the onset of in-line motion;
- 2.0 for maximum amplitude in-line motion;
- 3.5 for the onset of cross-flow motion;
- 5.5 for maximum amplitude cross-flow motion;

f_N is the natural frequency of the member, in Hertz (Hz);
W_S is the diameter of the pile, in metres (m).

In **Figure 24** and **Figure 25**, when the 40 mm and 30 mm piles were situated downstream of the 64 mm pile, they both oscillated at a lower frequency than what was expected. Whereas, the 64 mm pile did oscillate at its theoretical frequency. This could cause a potential issue during design when identifying the critical velocity of a pile situated downstream of a larger pile, even up to 10 diameters away. Since the piles oscillate with a lower frequency than expected, this results in the critical velocity being faster than calculated with **equation *(7)***. While this actually reduces the risk of failure, it could lead to the structure being over engineered, resulting in increased material and construction costs.

A similar situation could arise when designing downstream piles for steady drag force. **Figure 33** shows that when the 64 mm downstream pile was close to the upstream pile, it experienced more drag force than the upstream pile itself, which must be due to the wake and turbulence produced when the flow passes the upstream pile. The force steadily decreased until it levelled out around 9 to 10 diameters away, with a drag force very similar to that of the upstream pile. But, the force measured on the downstream pile 3 diameters away, was 1.47x greater than that on the upstream pile. If a structure is being designed in a river or estuary rather than out at sea, where the wave climate is small, the results show that piles within close proximity of each other may have to be designed to withstand larger drag forces than the steady drag formula suggests.

The results have clear implications on the installations of groups of piles. In certain predicable conditions, such as when a pile is located downstream of one of larger diameter, piles still experience lateral loading due to the cross-flow oscillations despite being situated behind another pile. The frequency of the oscillations of the downstream pile are not equal to the predicted frequency. Therefore, some form of bracing between the piles being installed immediately after the piles have been driven would reduce the chance of damage or even failure. This study has provided good answers to the original research objectives but has also provided good background information for further investigations. If this study was to be re-done or investigated further there are several changes that could be made and additional tests that could be done to improve the accuracy of the findings. These include;

- Rearranging the rig to minimise the shaking at higher current velocities but allow spacings of 1 and 2 diameters to be tested.
- Complete tests with the downstream pile further than 10 diameters away.
- Complete tests with more current velocities between 0.3 m/s and 0.7 m/s.

- Complete tests with a different diameter upstream pile, rather than keeping it at the largest diameter.
- Run each test twice to improve the reliability of the results.

Conclusions

In conclusion, the experiment has provided results that show how a pair of tandem piles in a current flow behave in both an in-line and cross-flow direction. The cross-flow oscillations caused by the shedding or vortices around the piles were measured with the strain gauges and analysed with MATLAB to calculate the frequency. A close relationship between the measured frequencies and the theoretical frequencies calculated with the pile Reynolds number and the Strouhal number was identified for a solitary pile of 3 different diameters, 64 mm, 40 mm and 30 mm. The oscillation frequencies of a pile downstream of the 64 mm pile were analysed to see what effect increasing the distance between the 2 piles had on the frequency of the oscillations. Initially, the downstream pile was also 64 mm in diameter and was incrementally moved from 3 to 10 diameters away. Tests were run with current velocities of 0.1, 0.3, 0.5, 0.7 and 0.9 m/s and the results showed that the frequency of the cross-flow oscillations closely matched that of the upstream pile, except in the case of the closest pile, 3 diameters away, where the frequency was slightly lower for all flow velocities. When the downstream pile was changed to the 40 mm and 30 mm pile the frequencies did not change as expected. Instead of frequencies close to the theoretical being measured for both the 40 and 30 mm downstream piles, they remained very similar to that of the upstream 64 mm pile. This occurred at all the tested flow velocities and spacings. This shows how the size of the upstream pile has a big effect on the movement of the downstream pile.

The results did not provide any evidence of a relationship between oscillation frequency and spacing between the piles at any flow velocity. The frequencies of the downstream pile remained roughly constant at all distances from the upstream pile. Although the size of the upstream pile influences what frequency the downstream pile oscillates at, the vortices shed by the upstream pile do not appear to influence the oscillations as they travel downstream. The in-line steady drag forces on the pile were also measured with strain gauges and analysed using MATLAB. However, due to the high sampling rate and sensitivity of the strain gauges causing lots of noise to be recorded, no clear results were found at current velocities of 0.1 and 0.3 m/s. Additionally, due to the set-up of the experiment the results at the higher flow velocities of 0.7 and 0.9 m/s also appear to be disrupted. This was due to way the piles were acting under the larger loads. The whole rig started to shake, and the piles violently vibrate, creating large forces through the strain gauges, much more than should have been experienced.

The results obtained from the 0.5 m/s tests clearly showed how the force decreased with distance from the upstream pile, with an increase above the force on the upstream being observed 3 diameters away. The force on the 40 mm and 30 mm piles decreased to less than the force on the upstream pile between 4 and 5 diameters away, while the force on the 64 mm pile remained greater than the force on the upstream.

Acknowledgments
Throughout the writing of this report I have received great assistance and guidance from my supervisor Dr Jon Miles. His expertise has been invaluable during the entire project from the initial proposal, during the experiment and with the writing of the report. I would like to thank my close friends and family for their continued support and for discussing my ideas and providing me with useful feedback. I would also like to thank Jacobs employees Ben Bullock and Rhys Bevan for taking the time to discuss my initial ideas with myself and Dr Jon Miles and for providing information and images about the Thanckes Oil Fuel Depot project.

References

Bevan, R (2019). *Driven piles at Thanckes Jetty* [Photograph].

British Standard Institution (2016). BS6349-1-2:2016: Maritime Works – General – Code of practice for assessment of actions. London: BSI Standards Limited.

Crowdy, D (2006). 'Analytical solutions for uniform potential flow past multiple cylinders', *European Journal of Mechanics B/Fluids*, 25, pp. 459-470.

Defence Infrastructure Organisation (2013). *Replacement Fuel Jetty and Fire Fighting System at Thanckes Oil Fuel Depot.* Available at: https://assets.publishing.service.gov.uk/government/uploads/system/uploads/attachment_data/file/252718/20131024-Thanckes-Exhibition.pdf (Accessed: 04 March 2019).

Department for Transport (2017). *UK Port Freight Statistics: 2017.* Available at: https://assets.publishing.service.gov.uk/government/uploads/system/uploads/attachment_data/file/762200/port-freight-statistics-2017.pdf (Accessed: 03 March 2019).

Engineers Edge (2019). *Water – Density Viscosity Specific Weight.* Available at: https://www.engineersedge.com/physics/water__density_viscosity_specific_weight_13146.htm (Accessed: 25 March 2019).

Fowler, A (2011). *Mathematical Geoscience.* London: Springer.

Hann, M (2018). 'Irregular and Random Waves'. *COUE318: Coastal Engineering Analysis and Design.* Available at: https://dle.plymouth.ac.uk/pluginfile.php/1169355/mod_resource/content/1/COUE318-507%20-%20Lecture%202%20-%20SV.pdf (Accessed: 09 April 2019).

Jacobs (2018a) Thanckes Oil Fuel Depot Loading Facility and Tank Farm Fire Fighting Upgrade: *Drawing 699810-CH2-00-JH-DR-C-3010 General Arrangement*. Jacobs, Swindon, UK.

Jacobs (2018b) Thanckes Oil Fuel Depot Loading Facility and Tank Farm Fire Fighting Upgrade: *Drawing 699810-CH2-00-JH-DR-C-3200 Jetty Head Pile Layout and Schedule*. Jacobs, Swindon, UK.

McDonald, G (2017) 'New £43m jetty to be built at Devonport naval base fuel depot' *Plymouth Live*. 24 October.

Miles, J. et al (2017) 'Current and wave effects around windfarm monopile foundations', *Coastal Engineering*, 121, pp. 167-178.

Mwaniki, A (2018) *The Busiest Cargo Ports in The United Kingdom.* Available at: https://www.worldatlas.com/articles/the-busiest-cargo-ports-in-the-united-kingdom.html (Accessed 08 March 2019).

Oka, S. et al (1972) 'Investigation of the heat transfer processes in tube banks in cross flow', *International Seminar on Recent developments in heat exchanges.* Trogir Yugoslavia.

Omega (2019) *Precision Strain Gage.* Available at: https://datasheets.globalspec.com/pdf/viewpdf?partId={6CE893C5-DB06-431E-87BB-3DAF3259A39B}&vid=99786&comp=580&r=1&from=detail (Accessed: 21 March 2019).

Sainsbury, R. N (1971) 'The flow induced oscillations of marine structures', *Proceedings of the Institution of Civil Engineers*, 49(3), pp. 269-302.

A.V. Oppenheim, R.W. Schafer (1975) Digital Signal Processing, Prentice Hall, New Jersey.

Sunden, B (2011) *Vortex Shedding*. Available at: http://thermopedia.com/content/1247/ (Accessed: 13 November 18).

Tomlinson, M (2007). Pile Design and Construction Practice. 5th Edn. CRC Press: Baton Rouge.

UK Ports (2018) *About UK Ports.* Available at: http://www.ukports.com/about.php (Accessed: 03 March 2019).

Whitehouse, R (1998). *Scour at Marine Structures: A manual for practical applications*. London: Thomas Telford.

Xu, G. Zhou, Y (2004) ‘Strouhal numbers in the wake of two inline cylinders’. *Experiments in Fluids*, 37, pp. 248-256.